International
Progress Report

IPR-01-02

Äspö Hard Rock Laboratory

Acoustic emission and ultrasonic monitoring during the excavation of deposition holes in the Canister Retrieval test

Will Pettitt and Calum Baker
Applied Seismology Consultants Ltd.

R Paul Young
Liverpool University

August 1999

Svensk Kärnbränslehantering AB
Swedish Nuclear Fuel
and Waste Management Co
Box 5864
SE-102 40 Stockholm Sweden
Tel 08-459 84 00
+46 8 459 84 00
Fax 08-661 57 19
+46 8 661 57 19

Äspö Hard Rock
Laboratory

Report no.	No.
IPR-01-02	F69K
Author	Date
Dr. W. Pettitt, Dr. C. Baker Prof. R.P. Young	99-08-10
Checked by	Date
Rolf Christiansson Jörgen Söderhäll	00-08-08
Approved	Date
Christer Svemar	01-03-16

Äspö Hard Rock Laboratory

Acoustic emission and ultrasonic monitoring during the excavation of deposition holes in the Canister Retrieval test

Will Pettitt and Calum Baker
Applied Seismology Consultants Ltd.

R Paul Young
Liverpool University

August 1999

Keywords: Acoustic emission, Canister Retrieval test, EDZ, Ultrasonic sound

Executive Summary

Two deposition holes have been excavated as part of the Canister Retrieval Test at the Hard Rock Laboratory, Sweden using a large diameter boring machine. The holes are 1.75m in diameter and 8.8m in length and were excavated in eleven 0.8m rounds. An ultrasonic array was installed around each deposition hole to investigate the response of the rock mass to the excavation. Acoustic emission (AE) monitoring has been used to delineate zones of stress-related fracturing around the deposition hole perimeter. Changes in ultrasonic velocities, measured every hour, have been used to investigate the response of the rock mass over a broader time and volume than the AE scale, and to quantitatively measure the accumulation of fracturing in the damaged zone.

AE locations from excavation of deposition hole DD0092G01 in the Canister Retrieval Test. (Figure 4-5)

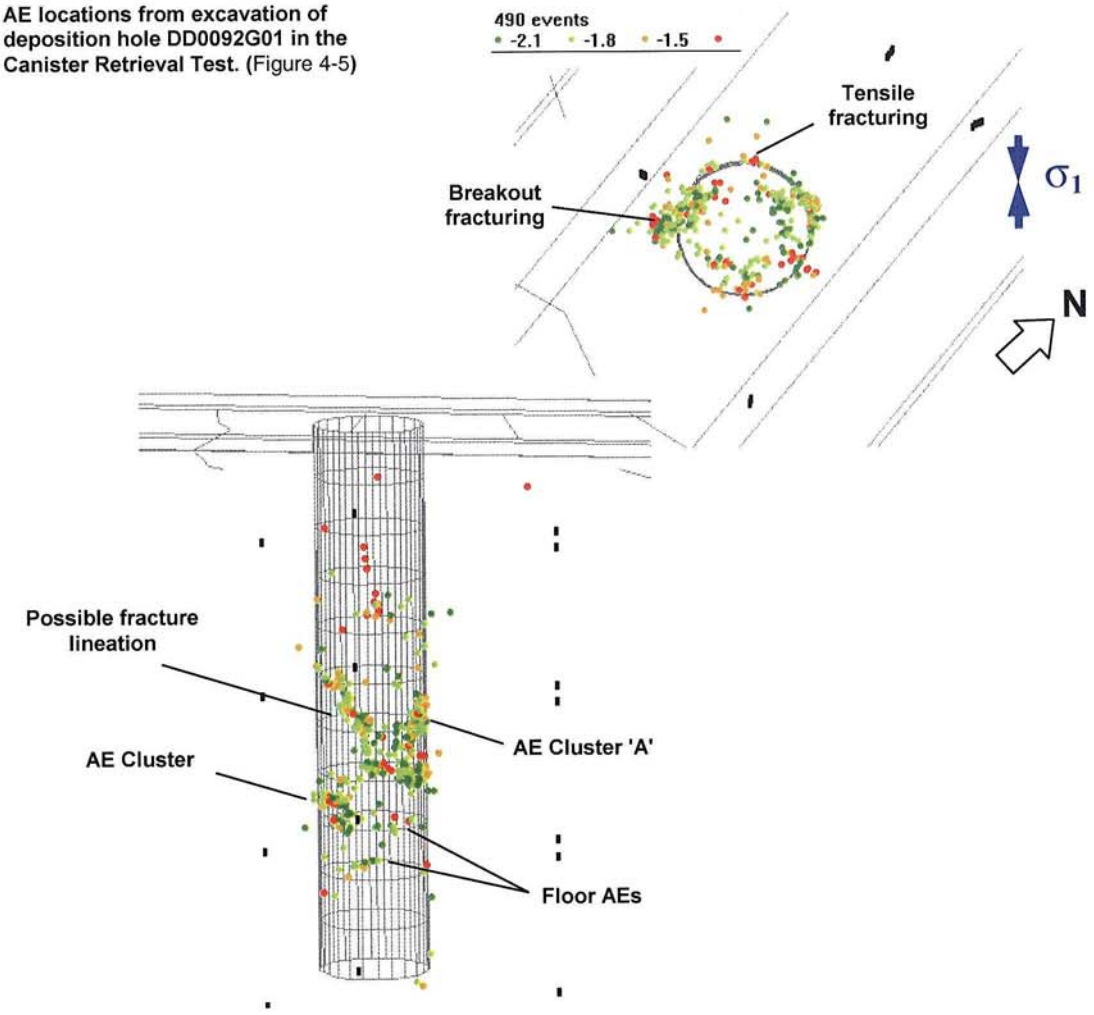

During the entire monitoring period there were a total of 2746 AE triggers. The AE results show regions of intense fracturing located in clusters down the deposition hole wall. These regions are orientated orthogonal to the maximum principal stress at the 420m level. The damaged zone is restricted to approximately 20cm from the deposition hole wall and activity decays rapidly within the first few hours after excavation. The clusters are probably a result of the interaction of induced stresses with excavation

through pre-existing features. A linear macroscopic fracture is also imaged. AEs are strongly time-dependent with fracturing being reinitiated around previous rounds when excavation of the deposition hole continues. AEs occur at a much reduced rate (<10 triggers per night) after completion of excavation. These effects are believed to be associated with stress redistribution in the pre-weakened regions.

Ultrasonic surveys give velocities for the pre-disturbed rock mass as approximately 5900m.s^{-1} for P-waves and 3350m.s^{-1} for S-waves. A 3% anisotropy has been imaged. These results are consistent with those obtained in ZEDEX. Surveys generally describe a drop in velocity during excavation. Observed changes vary from 4m.s^{-1} for ray paths at distance from the deposition hole to sharp drops of 20-30m.s^{-1} for ray paths skimming the deposition hole wall. These variations can be explained using a disturbed and a damaged zone model. As ray paths travel through the disturbed zone, in which induced stresses have preferentially opened or closed pre-existing microcracks, then the ray experiences small increases or decreases in velocity. This results in, for example, a 4m.s^{-1} change observed at distance from the deposition hole. However, ray paths skimming the deposition hole perimeter at 2-3cm distance pass through a region of accumulated damage close to the wall. These then experience a much sharper change in

Velocity change measured on the ray path illustrated in the right-hand margin. The red arrow shows the time at which excavation passed the ray path. (Figure 4-14)

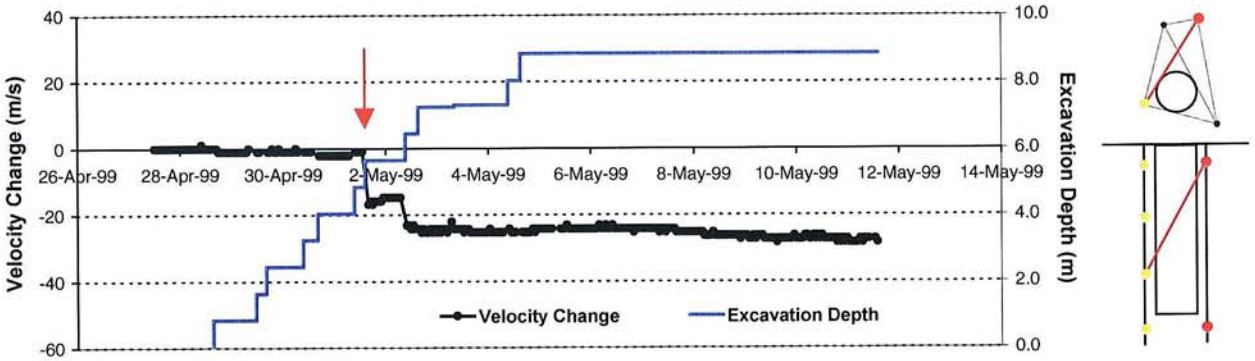

velocity of the order -15m.s^{-1} measured over the entire ray path. This corresponds to a 15% decrease in Young's modulus for the damaged zone.

A CD is included with this report presenting AE locations for the two deposition holes. The user can interactively step through the data in time and also control the view orientation and magnification.

Contents

List of Figures

List of Tables

1 Introduction

This report describes results from acoustic emission and ultrasonic monitoring of the excavation of two deposition holes (identified as DD0092G01 and DD0086G01) in the Canister Retrieval Test (referred to as CRT for the remainder of this report). The aim of the CRT is to illustrate that waste canisters can be safely retrieved from a repository underground environment. It is located at the 420m level in SKB's Hard Rock Laboratory (HRL), Sweden (Figure 1-1). Excavation of the two deposition holes was performed during the period 28th April to 3rd June 1999. Each hole has been bored vertically from the concrete floor of the tunnel and measures 1.75m in diameter and approximately 8.8m in length. Excavation was undertaken in eleven 0.8m rounds.

The rock mass at this level is predominantly massive Äspö diorite with sparse en-echelon fractures orientated in two main discontinuous sets; a northwest steeply dipping set is regarded as the main water-bearing set. Principal stresses are described in Table 1-1. An *in situ* stress ratio of 3:1 exists. The uniaxial compressive strength of the Äspö diorite is approximately σ_c=170MPa and a uniaxial crack-initiation stress is reported as σ_{ci}=64MPa [*Young et al.*, 1996]. Although stress magnitudes at the HRL are relatively small compared to the strength of the rock the effect of the tunnel in a simple Kirsch solution (e.g. *Young et al.*[1996]) is likely to increase the maximum compressive stress observed in the floor to as much as 80MPa. There is then an additional effect of stress distribution around the large deposition holes. This multiplication of stresses may result in stress-induced fracturing around the perimeter of the holes. Similar observations have been made at AECL's Underground Research Laboratory (URL), Canada (e.g. *Read and Martin*[February 1996]), although in this case the *in situ* stress ratio is approximately 6:1.

Stress Component	Magnitude (MPa)	Trend (°)	Plunge(°)
σ_1	32	131	0
σ_2	17	41	25
σ_3	10	229	65

Table 1-1: Principal stress values for the 420m level used by Young et al.[1996] and originally reported by Leijon[1995].

Ultrasonic monitoring has been shown to be an effective tool for observing induced fracturing and the response of a medium to applied stresses. *Falls and Young*[1998] gives a review of ultrasonic results from a number of excavation experiments conducted in different underground environments. In recent years hardware and processing software have been developed by the Applied Seismology and Rock Physics Laboratory at Keele University and now by Applied Seismology Consultants Ltd. (ASC), UK specifically for monitoring material changes due to stress-induced damage. Two techniques are utilised using the same monitoring equipment; acoustic emissions and ultrasonic surveying.

Acoustic emissions (AEs) are used to depict the localisation of brittle fracturing on the scale of millimetres in the rock mass. AEs are a time dependent phenomena. In this case, they may occur instantaneously as the deposition hole is excavated due to the method itself or due to the relaxation of the rock mass. They may also occur over a

longer period of time due to stresses distributed around the new void inducing new fracturing within the rock or causing disturbance of any pre-existing fractures that may exist. Ultrasonic velocity measurements are used to quantitatively measure the response of the rock over a broader volume and time than the AE scale. Measurements are sensitive to the closing and opening of fractures due to changes in the stress field and due to the accumulation of induced damage within the rock volume. By combining AE measurements, localising the extent of induced damage, and ultrasonic measurements, quantifying the degradation of the rock mass, it is then possible to measure the overall disturbance induced by both the excavation method and the *in situ* stresses acting on the new void.

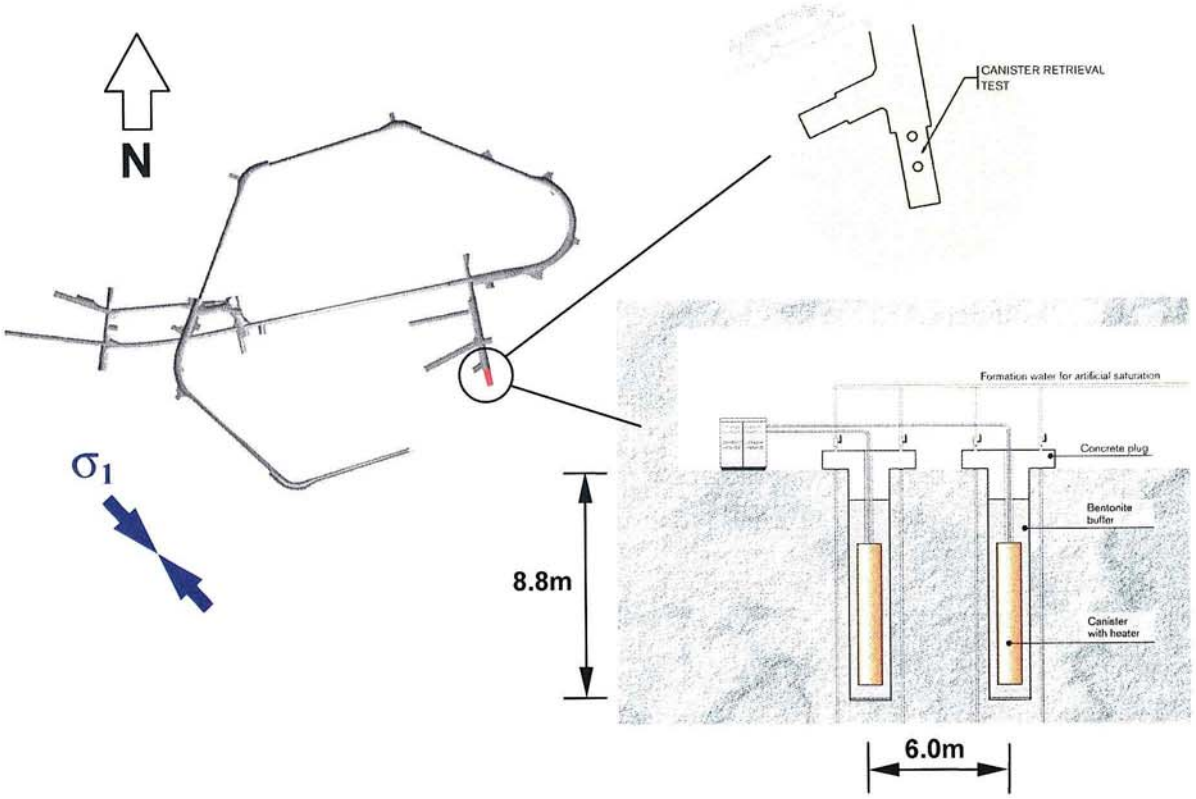

Figure 1-1: *Plan view of the experimental tunnels at the Äspö HRL and the location of the CRT. A schematic illustration of the final CRT experimental set up is shown with canisters and bentonite clay installed in the two 1.75m diameter deposition holes. Graphics are modified from SKB[1999].*

2 Experiment Objectives

Acoustic emission and ultrasonic monitoring of the deposition hole volume has been conducted in the period 26th April to 12th June 1999 with the following objectives.

- Monitor the background acoustic emission (AE) activity within the deposition hole volume prior to excavation, and perform ultrasonic surveys so as to determine the background ultrasonic velocity in the volume.

- Monitor AE activity immediately after excavation of each deposition hole round, and for a period after completion of each deposition hole. Produce accurate source locations for AEs so as to delineate the spatial and temporal extent of brittle microcracking within the surrounding rock mass and the effect of excavation on pre-existing macroscopic fractures.

- Conduct regular ultrasonic surveys during the excavation period so as to observe the ultrasonic response of the rock mass around the deposition hole as excavation commences. In particular this should use ray paths that skim the perimeter of the deposition hole so as to have a sensitive measure of the excavation response within the immediate rock mass. Use ultrasonic velocities to produce a measure of damage accumulation in this region.

3 Methodology

3.1 Data Acquisition

The ultrasonic array consists of twenty-four ultrasonic transducers mounted in four borehole sondes (Figure 3-1). Each sonde contains two transmitters and four receivers (Figure 3-3). The sondes are installed in vertical 76mm diameter boreholes approximately 10 meters in length distributed around each deposition hole volume (see Section 3.2 for array geometry). The sondes are fixed to the borehole collars using small bolted steel attachment rods and steel plates are fixed over the borehole collars for protection. The sensors are spring loaded against the borehole wall so as to produce good coupling to the rock (Figure 3-2). The transducers respond to the frequency range 35-350kHz.

The piezoelectric transducers operate by converting a passing elastic wave into an electric signal or visa versa. The monitoring system is then operated in one of two modes. The first is used to passively monitor AE activity preferentially within the array volume. AEs release elastic energy in the same way as 'earthquakes' but over a very small scale. At these frequencies AEs have a moment magnitude (M_w) of approximately -6. They occur either during the creation process of new fractures within the medium, or on pre-existing fractures due to small scale movements. Signals from the receivers are first amplified by 40dB and are then captured by an ESG Hyperion Acquisition System controlled by a PC (Figure 3-1). An AE is recorded when the amplitude of the signal on a specified number of channels exceeds a trigger threshold within a time window of 5ms. The system then records the signals from all 16 transducers. In this case a trigger threshold of 50mV on three channels was used. This allows the system to have sufficient sensitivity to record high quality data without recording an abundance of activity that cannot be processed due to very small signal to noise on only a few channels. The captured signals are digitised with a sampling interval of 1μs and a total length of 4096 data points. In general, low noise levels were observed (<2mV) giving high signal to noise and good quality data. Example waveforms from an AE are given in Figure A1.

The second operating mode actively acquires ultrasonic waveforms by scanning across the volume. This allows measurements of P- and S-wave velocities and signal amplitudes over a possible 128 different ray paths. By repeating these ultrasonic surveys at increments of time, a temporal analysis can be obtained for the variation in medium properties. A Panametrics signal generator is used to produce a high frequency electric spike (Figure 3-1). This is sent to each of the 8 transmitters in turn. The signal emitted from each transmitter is recorded over the 16 receivers in a similar fashion to that described above. An external trigger pulse from the signal generator is used to trigger the acquisition system and identifies the transmission start time to an accuracy of one sample point. In order to decrease random noise the signal from each transmitter is stacked 100 times. Example waveforms from an ultrasonic survey are given in Figure A2.

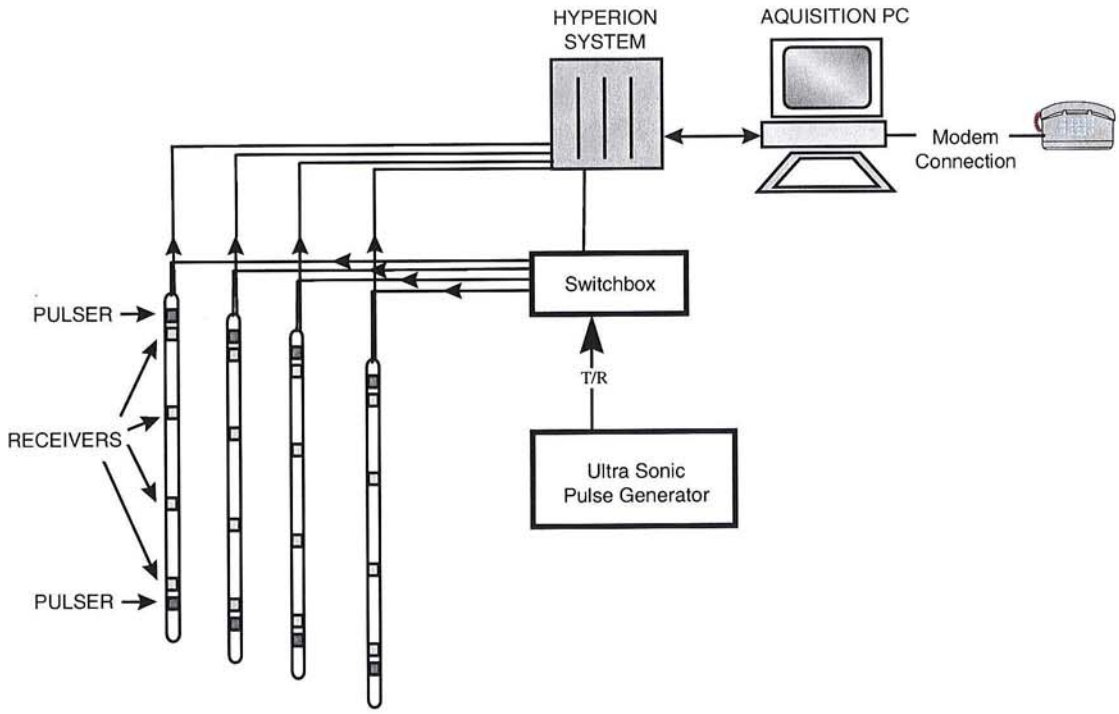

Figure 3-1: *Schematic diagram of the hardware used in the CRT. The ultrasonic pulse generator sends a signal to each transmitter and the resulting signal is recorded on each receiver. The receivers are also used to listen for AE activity.*

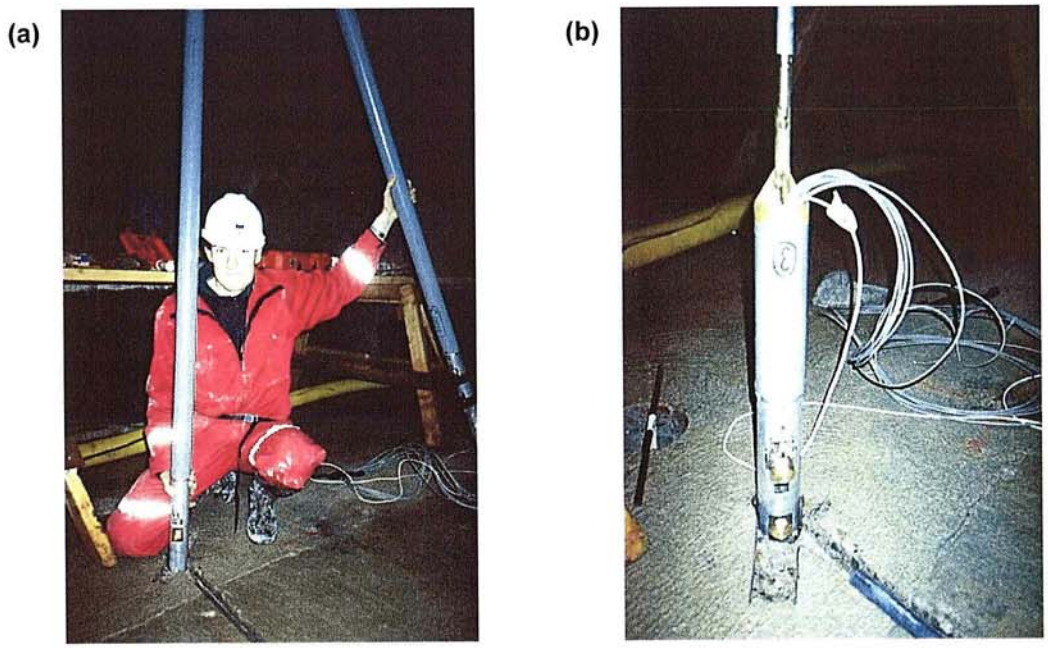

Figure 3-2: *Photographs showing installation of one of the four 8m long borehole sondes used for ultrasonic monitoring. Photo b) shows the upper two transducers, the uppermost being a transmitter and the lower a receiver (e.g. Figure 3-3). Brass caps are fixed over the transducer faces to give good coupling to the borehole wall.*

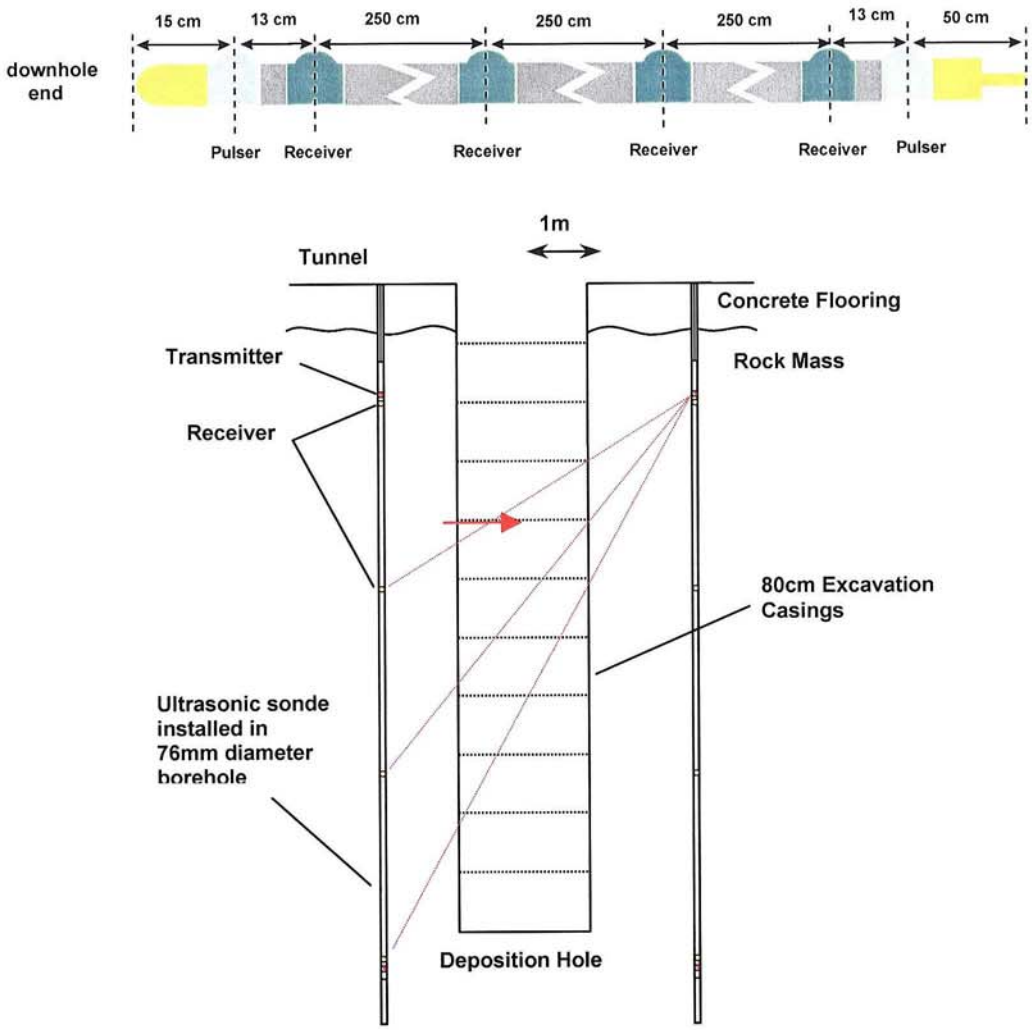

Figure 3-3: Top: *Design of the borehole sonde used during ultrasonic monitoring of deposition holes; a transmitter is located at each end of the sonde and four receivers are equally spaced at 2.5m intervals.* ***Bottom:*** *Illustration of the array after installation; sondes are placed in 10m long vertical boreholes. Excavation of the deposition hole is in eleven 80cm rounds/casings. The red arrow indicates the 'passing depth' used in Section 4.3 and is defined as the excavation depth at which the deposition hole passes nearest to the shown ray path.*

3.2 Array Geometry

The sonde locations for each deposition hole are described in Figure 3-4 and in **Fel! Hittar inte referenskälla.** and **Fel! Hittar inte referenskälla.**. The array geometry has been designed so as to monitor the complete perimeter of each deposition hole and to produce 'skimming' ray paths during ultrasonic surveys. These ray paths pass within a few centimetres of the deposition hole wall and hence through a region most likely to experience excavation damage. The same four borehole sondes have been used for each array having been re-installed between excavations. Each sonde has been accurately orientated so that the sensor caps point towards the axis of the monitored deposition hole.

Sonde #.	Borehole Ref.	Transmitter #.	Receiver #.
1	KD0089G01	1, 2	1-4
2	KD0089G02	3, 4	5-8
3	KD0094G01	5, 6	9-12
4	KD0092G02	7, 8	13-16

Table 3-1: Location of ultrasonic array for monitoring of deposition hole DD0092G01. See Figure 3-4 for illustration of array geometry.

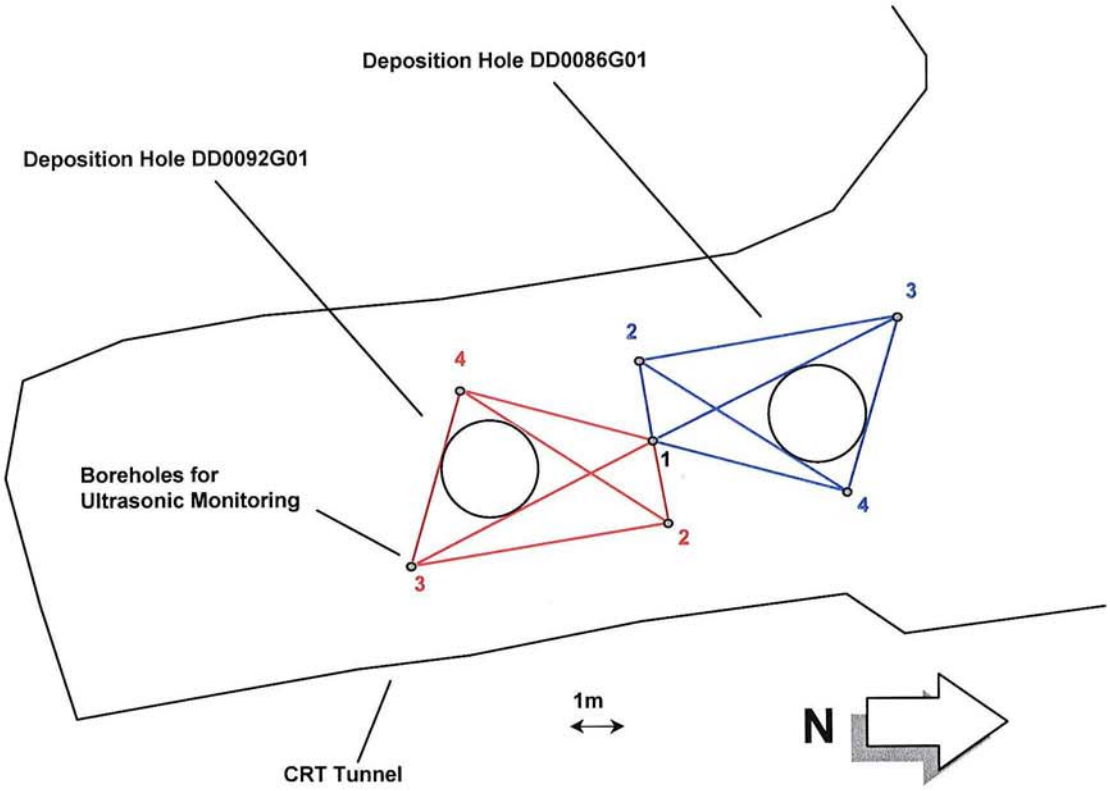

Figure 3-4: *Plan view of the array geometries for the two deposition holes, DD0092G01 and DD0086G01 excavated in the CRT. Red labels are borehole locations for monitoring of deposition hole DD0092G01 labelled by Sonde # (**Fel! Hittar inte referenskälla.**). Blue labels are borehole locations for monitoring of deposition hole DD0086G01 (**Fel! Hittar inte referenskälla.**). Red and blue lines are direct ray paths between sondes illustrating their 'skimming' nature.*

Sonde #.	Borehole Ref.	Transmitter #.	Receiver #.
1	KD0089G01	1, 2	1-4
2	KD0089G03	3, 4	5-8
3	KD0084G01	5, 6	9-12
4	KD0086G02	7, 8	13-16

Table 3-2: Location of ultrasonic array for monitoring of deposition hole DD0086G01. See Figure 3-4 for illustration of array geometry.

3.3 Monitoring Procedure

Ultrasonic monitoring started three days before the start of drilling of each deposition hole, and continued for a number of days after the finish of drilling (Figure 3-5). Monitoring was performed 24 hours per day except during any times of high frequency noise in the rock volume (e.g. deposition hole drilling). During each drilling increment (round), the acquisition system was switched off immediately after the start of excavation and switched on just before the completion of excavation. Immediately after each round a two hour quiet period was observed in the tunnel when no maintenance could be performed on the drilling machine. This period was used for AE monitoring. AE monitoring was also performed overnight between the hours of 2000 to 0600 and during daytime hours when activity on the drilling machine was known due to the system operator being on site.

Ultrasonic surveys were conducted hourly so as to obtain high temporal resolution in the P- and S-wave velocity and amplitude variation along transmitter-receiver ray paths. Surveys were not conducted during deposition hole excavation due to drill noise, and during the first hour of AE monitoring after cessation of drilling.

A calibration survey was performed in each deposition hole so as to analyse uncertainties in AE locations and to calibrate the location algorithm. A mechanical ultrasonic source (Schmidtt hammer) was used in known locations around the deposition hole interior when access permitted. Surveys were performed a few days after the finish of drilling of deposition hole DD0092G01 (11th May 1999) and when excavation was at 3.22m depth for deposition hole DD0086G01 (20th May 1999).

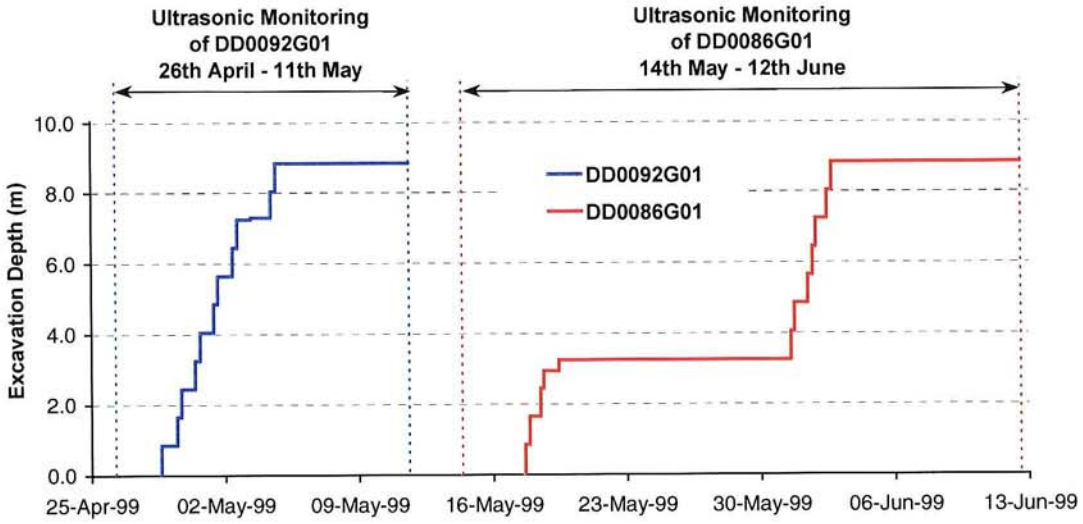

Figure 3-5: *Time chart illustrating the monitoring periods for excavation of the two deposition holes in the CRT.*

3.4 Processing Procedure

Data formats and storage procedures are described in *ASC*[1999]. The raw data are stored as 'events', each being 16 recorded waveforms. The events contain the following data types.

- Microcrack induced acoustic emissions (AEs)
- Ultrasonic survey recordings
- Machine drill noise
- Machine maintenance noise

The first stage of the processing is to split these types into individual data sets. The complicating factor in this experiment has been the occurrence of significant amounts of machine drill and maintenance events occurring sporadically in time and mixed in with the AE events. It is highly important that this noise is removed so that spurious 'AEs' are not described in the results. To do this the machine data logger was repeatedly synchronised in time with the ultrasonic monitoring system. The time of completion of each excavation round was then logged to an accuracy of approximately 5 seconds. Periods of machine maintenance were also logged. The time of every potential AE trigger was then manually inspected to see if it occurred within a known quiet period when no such noise was occurring. All potential noise was discarded.

AE data and ultrasonic surveys from each deposition hole have then been processed independently and contain the following steps.

Ultrasonic surveys:

1. One survey from each deposition hole is manually picked for P- and S-wave arrival times where possible. The uncertainty in any P-wave time measurement is approximately ±3μs. Velocities are calculated using the time of flight between known transmitter and receiver locations. Uncertainties in P-wave velocity measurements are approximately ±30m.s^{-1}.

2. P- and S-wave arrival times for each hourly survey during the monitoring period are then measured using a cross-correlation procedure. This gives a much more precise measurement of velocity variation than manual processing allows. Thus allowing small (<30m.s^{-1}) velocity changes to be observed. It also allows the efficient processing of large volumes of data. The manually processed survey acts as a reference survey. The arrivals for every survey are first obtained using an automatic picking algorithm. A data window is then formed around each arrival and the window is then cross-correlated with a similar window from the reference survey. This gives a measurement of the change in arrival time to an accuracy of ±0.2μs. The change in time is then used to calculate a change in velocity with an estimated uncertainty of ±2m.s^{-1}.

3. P- and S-wave RMS signal amplitudes are also obtained from data within a fixed time window around the arrivals.

Acoustic emissions:

1. Calibration surveys are used to optimise an automatic picking and source location algorithm and check location uncertainties.

2. Where possible, P- and S-wave arrival times are measured for each AE using the automatic picking procedure.

3. AEs with ≥6 P-wave arrival times are input into a downhill-simplex location algorithm. This has the option of incorporating either a three-dimensional anisotropic velocity structure or an isotropic structure. Velocities calculated from the ultrasonic surveys are used. It also has the option to constrain locations to lie outside of known voids.

4 Results from Ultrasonic Monitoring

4.1 Ultrasonic Velocity Structure

Reference ultrasonic surveys have been chosen from the period before excavation began for each deposition hole so as to obtain a measure of the background velocity structure. P-wave velocity measurements for deposition hole DD0092G01 are shown in the lower-hemisphere stereonet of Figure 4-1a. The mean velocity is 5903m.s^{-1} over 64 ray paths. The scale range in this plot is 5740-6100m.s^{-1} and each colour increment varies by the estimated uncertainty in any one measurement (30m.s^{-1}). A weak anisotropy is observed between a minimum 5800m.s^{-1} and a maximum 6020m.s^{-1}, or approximately 3%. A three-dimensional anisotropy model for the data is presented in Figure 4-1b constructed using the method of *Falls*[1993]. This shows the fast direction to be orientated at approximately 280° East of North and with a plunge of 40° from the horizontal. A similar result is obtained for deposition hole DD0086G01 (Figure A4). In this case a mean velocity of 5914m.s^{-1} over 70 ray paths is observed. The velocity magnitudes obtained in this study are in very close agreement with that obtained at ZEDEX [*Falls and Young*, May 1995; *Falls and Young*, October 1994] although the anisotropy direction is slighted rotated towards the horizontal.

There are two mechanisms which could explain the anisotropy. It should be noted that the velocity must depend upon a variation in physical structure much smaller than the array dimension of approximately 5x5x8m. The velocity could then depend upon a pre-existing fracture fabric or grain alignment. This would be orientated NE-SW with a plunge of 40°NW. The anisotropy could also depend upon the orientation of the maximum principal stress, σ_1 as this will act to preferentially close fractures orientated orthogonal to this direction. There is a reasonably close association between σ_1 and the observed fast direction (Figure 4-1b).

The mean S-wave velocity for deposition hole DD0092G01 has been measured as 3350m.s^{-1} and for deposition hole DD0086G01 as 3301m.s^{-1}. Measurements generally ranged from 3200-3400m.s^{-1} with an estimated uncertainty of 60m.s^{-1}. These values give a dynamic Poisson's ratio of 0.26. This agrees with dynamic Poisson's ratios observed for Lac du Bonnet granite at the URL, Canada (e.g. Read and Martin

February 1996]).

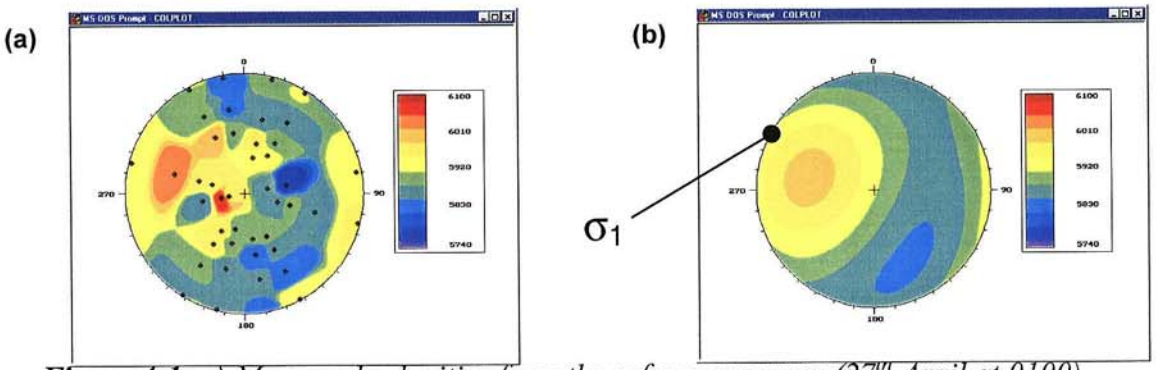

Figure 4-1: a) *Measured velocities from the reference survey (27th April at 0100) used for deposition hole DD0092G01.* ***b)*** *Three-dimensional anisotropy fit to the data.*

4.2 Acoustic Emissions

There were 1531 system triggers during monitoring of the deposition hole volume DD0092G01 that are associated with valid AEs. There were 1215 during monitoring of deposition hole volume DD0086G01. However, many of these AEs (approximately 66%) have produced unconstrained locations. In this section we only present data we believe have uncertainties <10cm and hence give a realistic and accurate view of permanent damage associated with deposition hole excavation.

Two-thirds of the data is unlocated due to the deposition hole being large compared to the monitoring array. As the deposition hole is excavated deeper, the void begins to shadow regions of the rock mass from some of the recording transducers. Signals from AEs that occur within these regions become greatly attenuated when travelling to shadowed transducers. Hence, fewer arrival times can be picked accurately. When signals are recorded on shadowed transducers they include an additional travel time for the ray path bending around the deposition hole volume. This shadow effect then results in locations being pushed away from the deposition hole perimeter and floor and into the rock mass. Figure A5a and Figure A6a show locations of calibration shots from within the two deposition holes, and using all available travel time picks. The locations observed ultrasonically (red markers) are sometimes very different to the actual shot locations (green markers). We have solved this problem by automatically removing ray paths that are considerably effected by the deposition hole. Figure A5b and Figure A6b show the same calibration shots but located without these ray paths. A considerable improvement in the locations is made. Locations now have an estimated uncertainty of ±9cm.

This method should not adversely effect the distribution of locations around the deposition hole perimeter as generally travel times from only a few transducers will be lost. However, the method does effect the sensitivity of the processing to locations beneath the floor of the deposition hole. AEs beneath rounds at large depth are more

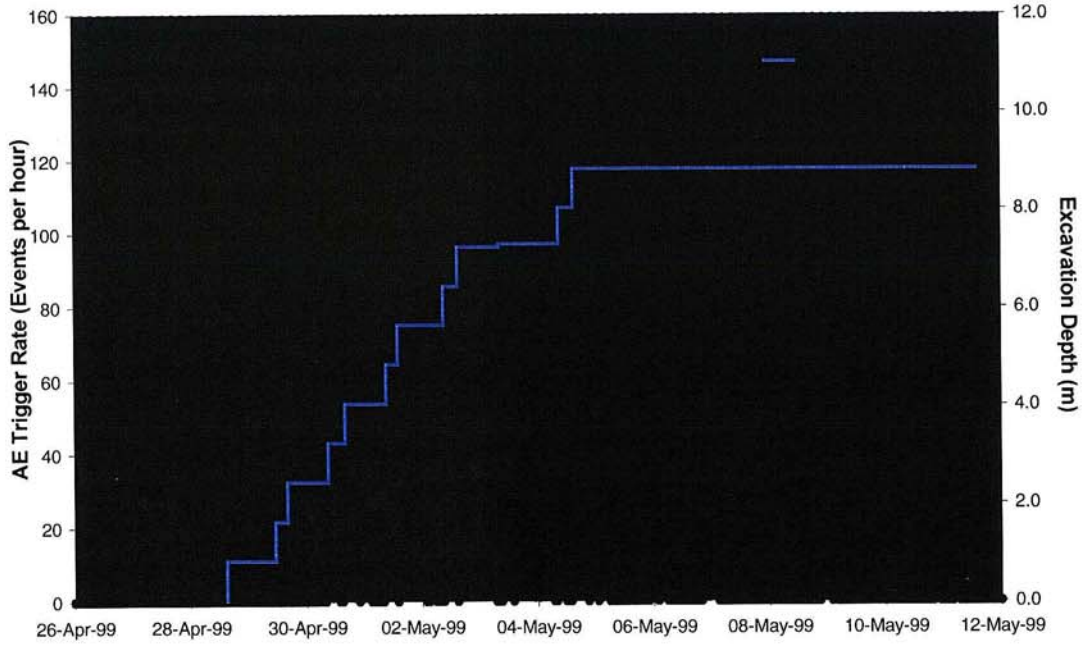

Figure 4-2: *AE trigger rate through excavation of deposition hole DD0092G01. The excavation depth is also shown.*

likely to be removed from the data set as a larger number of travel times become

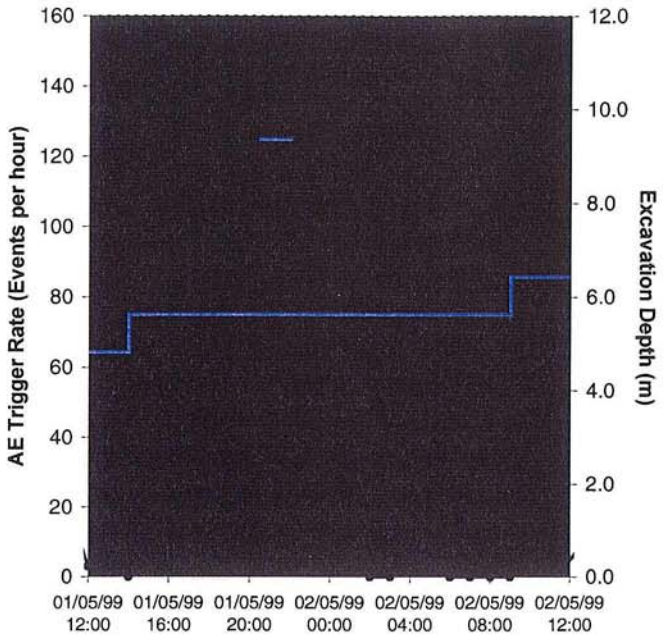

Figure 4-3: *Time expansion of Figure 4-2 for monitoring of post-round #7 (excavation depth = 5.63m).*

effected by the deposition hole volume. As the floor of each round is removed by excavation of the subsequent round then an analysis of this data is less important than that located in the deposition hole walls.

Figure 4-2 shows the AE trigger rate for deposition hole DD0092G01. Activity within the deposition hole volume before excavation began was negligible (1 trigger in 3 days of monitoring). The most abundant activity (up to 160 triggers per hour) was observed during the period 1st-4th May when excavation of rounds 6 through to 9 (4.83-7.23m) was performed. Activity from the first five rounds is small in comparison (up to 50 triggers per hour). Figure 4-3 shows the trigger rate from round #7. In this case there were 14 hours of continuous monitoring post-excavation during which no machine noise caused a problem. As can be seen the activity decays rapidly over four hours from 150 triggers per hour to approximately 10 triggers per hour. The decay continues so that after 12 hours there are only 2-4 triggers per hour maximum. After completion of the entire excavation, activity quietens within the first 24 hours to a consistent 5-10 triggers per night (Figure 4-2). The response of the rock mass is therefore reasonably rapid and there is no abundance of fracturing continuing after excavation of the complete deposition hole. This contrasts significantly with that observed at higher stress regimes where activity continues at a much higher rate for many months (e.g. *Young and Collins*[1999]).

The fact that the amount of activity in the first 4m of excavation is smaller is probably related to induced stresses increasing as the deposition hole becomes deeper. Similar AE observations have been made for large diameter boreholes at the URL [*Falls and Young*, 1998]. At depths greater than 4m induced stresses have become sufficient to cause the observed fracturing. Figure 4-5 shows 490 constrained locations for deposition hole DD0092G01. The locations occur very close to the deposition hole perimeter and in particular in two breakout regions orthogonal to σ_1. Figure 4-4a shows the distribution of AE numbers with azimuth around the deposition hole perimeter. The AEs are tightly distributed at approximately 90° to σ_1. This is in regions of the rock mass that would be expected to have high-magnitude compressional stresses in a simple Kirsch solution. Figure 4-6 highlights the observed breakout regions. AEs are fewer, although not non-existent, parallel to σ_1 and very close to the deposition hole wall. These occur in regions of low compressional stress or tensile stress.

Figure 4-4b describes how far the damage extends into the deposition hole wall. It's observed that >70% of the AEs occur in the first 10cm and >90% in the first 20cm. It's therefore reasonable to assume that the damage region only extends to approximately 20cm. AE locations in Figure 4-5 are observed in distinct clusters down the deposition hole. Stress-induced damage is hence not continuous down its length. These clustered regions probably occur where the rock wall has been already weakened, either by the excavation process and/or the existence of pre-existing features. The crack-initiation stress in these regions may then be reduced and induced stresses increased such that permanent damage results.

Figure 4-7 shows all AEs located during the excavation of rounds 5 to 7. The AEs distinguish a zone of activity that seems to be associated with a linear feature intersecting the deposition hole. These AEs locate both in the wall of the deposition hole and in the floor of each round. The feature is orientated with a strike of 70o East of North and a dip of 50oNNW. This is a similar orientation to the anisotropy observed in Figure 4-1. Figure 4-9 describes the time dependency of the observed AEs. Activity is prolonged in the round 6-9 volume, occurring for the remainder of the excavation. Particularly active is the round 6 volume and one cluster of activity marked as 'A' in Figure 4-5. The small number of triggers recorded after the complete excavation are generally associated with this cluster.

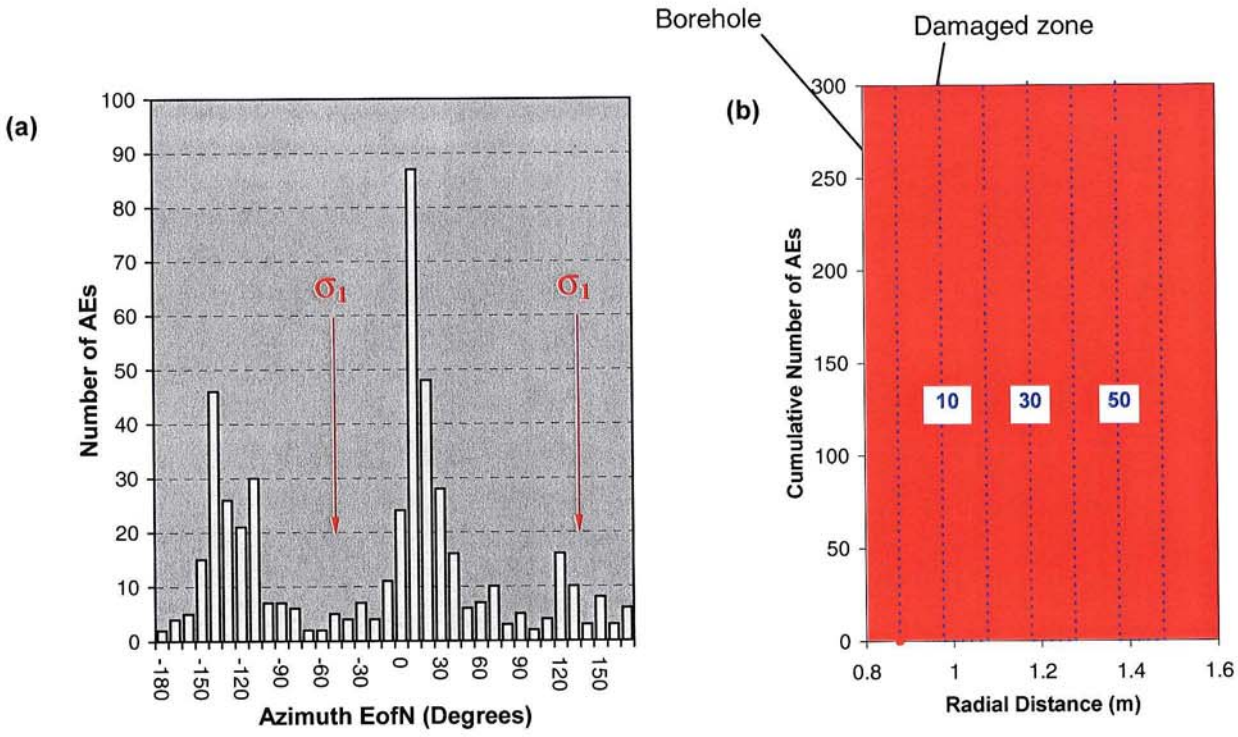

Figure 4-4: a) *Number of located AEs versus azimuth around the perimeter of deposition hole DD0092G01. The red arrows indicate the orientation of* σ_1. ***b)*** *The cumulative number of AEs locating outside of the deposition hole perimeter with radial distance. Blue dashed lines and labels indicate distance from the deposition hole wall.*

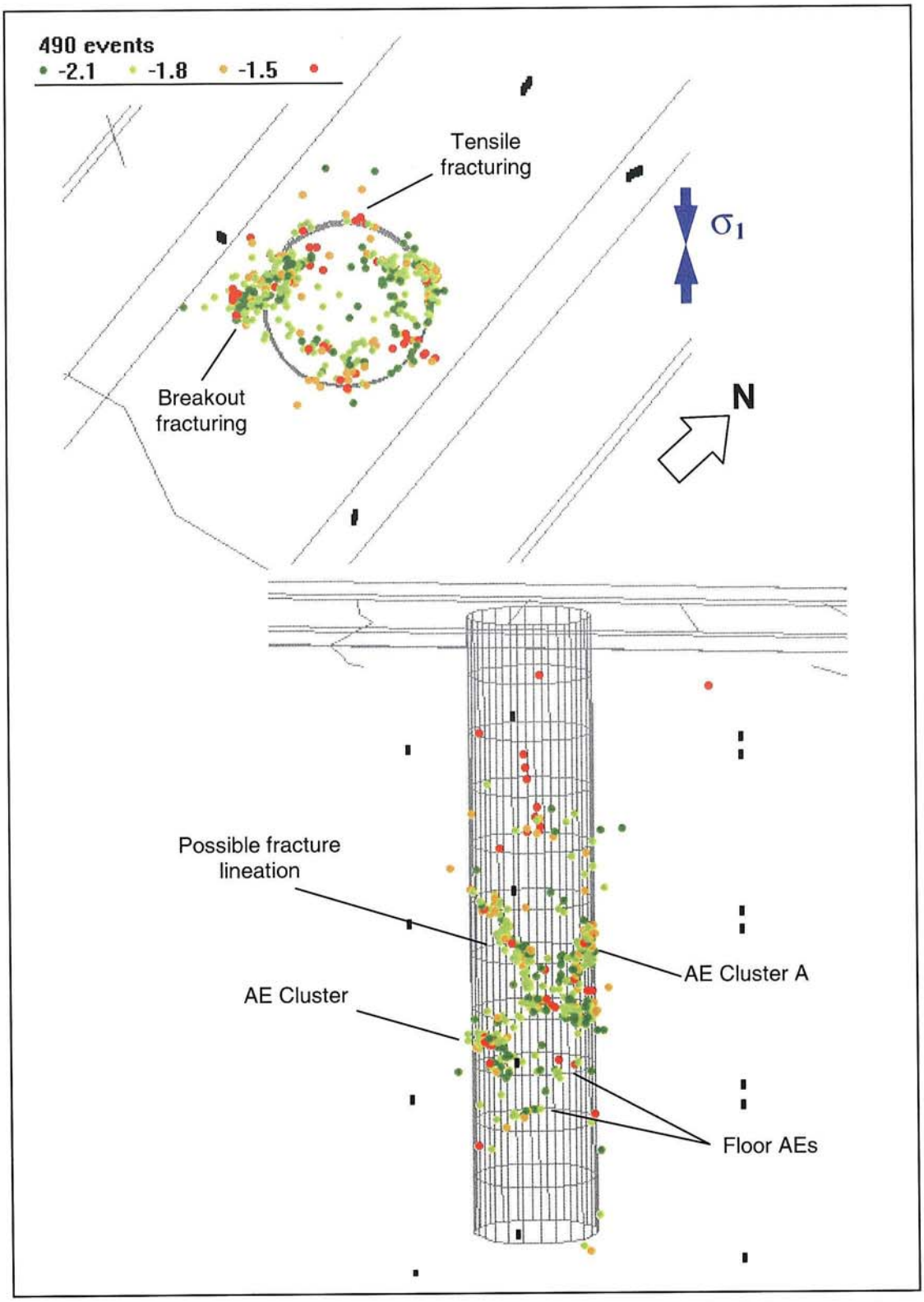

Figure 4-5: *AE locations from monitoring of deposition hole DD0092G01. The marker colour indicates the relative ultrasonic magnitude. The upper view is in plan and is rotated such that σ_1 is up the page. Lower plot is viewed at an azimuth of 260° East of North and with a plunge of 10° from the horizontal. Black markers show transducer locations.*

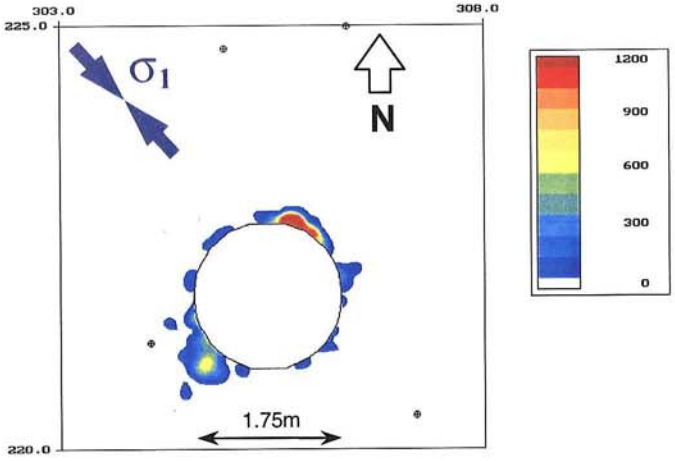

Figure 4-6: *An AE density plot (plan view) for deposition hole DD0092G01. Also shown is the σ_1 direction. Units are interpolated number of AEs per m^2.*

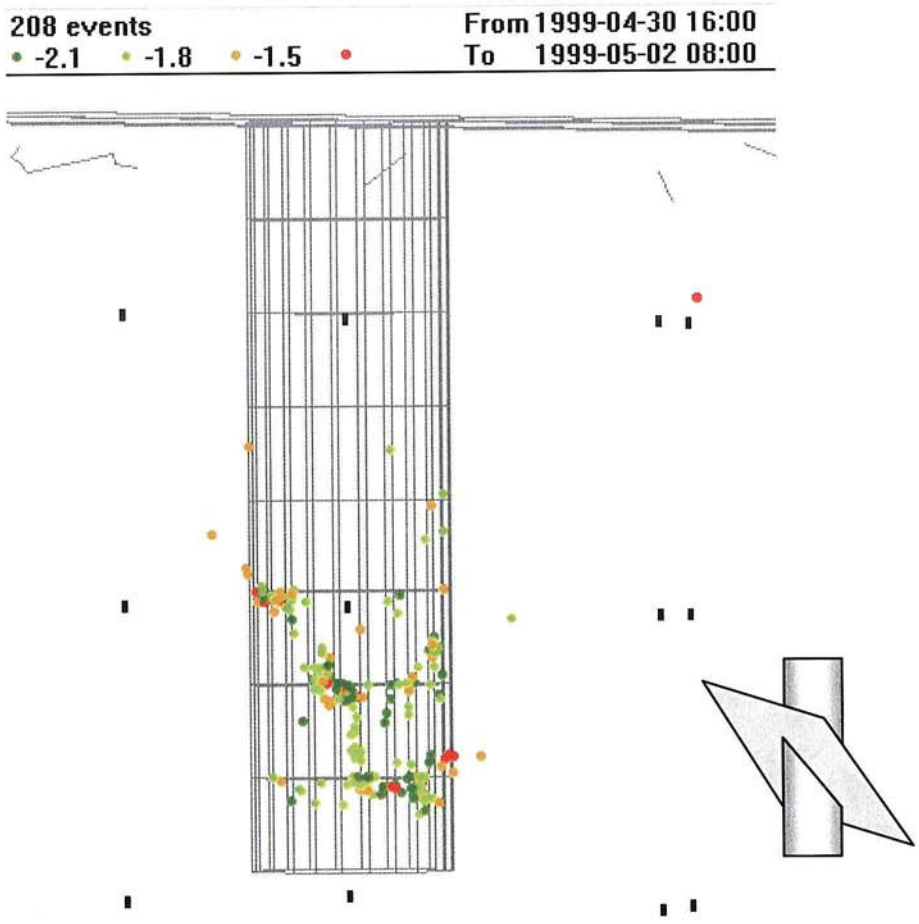

Figure 4-7: *AE localisation of a possible pre-existing feature intersecting the perimeter of deposition hole DD0092G01. The data shown is from the monitoring of rounds 5 to 7. The view is approximately along strike.*

The pattern of activity is not as distinct for deposition hole DD0086G01 as for the first deposition hole. In this case, AEs occur at a much reduced rate (Figure A8). The total number of triggers is reduced by 20% and the activity rate never passes beyond 80 triggers per hour, unlike the first deposition hole where the activity was observed to be as large as 160 triggers per hour. However, AE distributions associated with breakout fracturing orthogonal to σ_1 are still apparent (Figure 4-10). Again there are also minor amounts of AEs parallel to σ_1 possibly caused by tensile stresses in this region.

In this case, the activity appears to locate at slightly shallower depths than previously with the majority of AEs locating in rounds 2 to 7 or 1.5-4.5m depth (Figure A11). Although minor clustering is observed there is not the large clusters of activity that were observed in the previous deposition hole. Instead, the AEs are more diffusely located down the deposition hole length. The locations are also asymmetric relative to the deposition hole axis giving the impression of a 2m wide band of activity. Again this damaged region is close to the perimeter of the deposition hole although it may extend further into the rock mass than previously; 75% of the AEs occur in the first 30cm. These location differences could be caused by the stress field being dissimilar to the previous case and/or pre-existing features that caused localisation of activity around the first deposition hole being fewer in number. The activity observed in the round 2 to 7 region is strongly time dependent (Figure A7). There is a large time gap during excavation of the deposition hole between 19th-31st May 1999, after completion of round #4 (Figure 4-10 shows the activity up to and including the excavation of this round). During this time the triggers decay to 1-2 per night. AEs during this period are located along the 3.22m length of the deposition hole. When excavation begins on the fifth round AEs are initiated not only in the round 5 volume but also at shallower depths. This is a similar effect to that observed in the first deposition hole and is a strong indication of stress-induced fracturing occurring as the stress field is further perturbed by the continuing excavation.

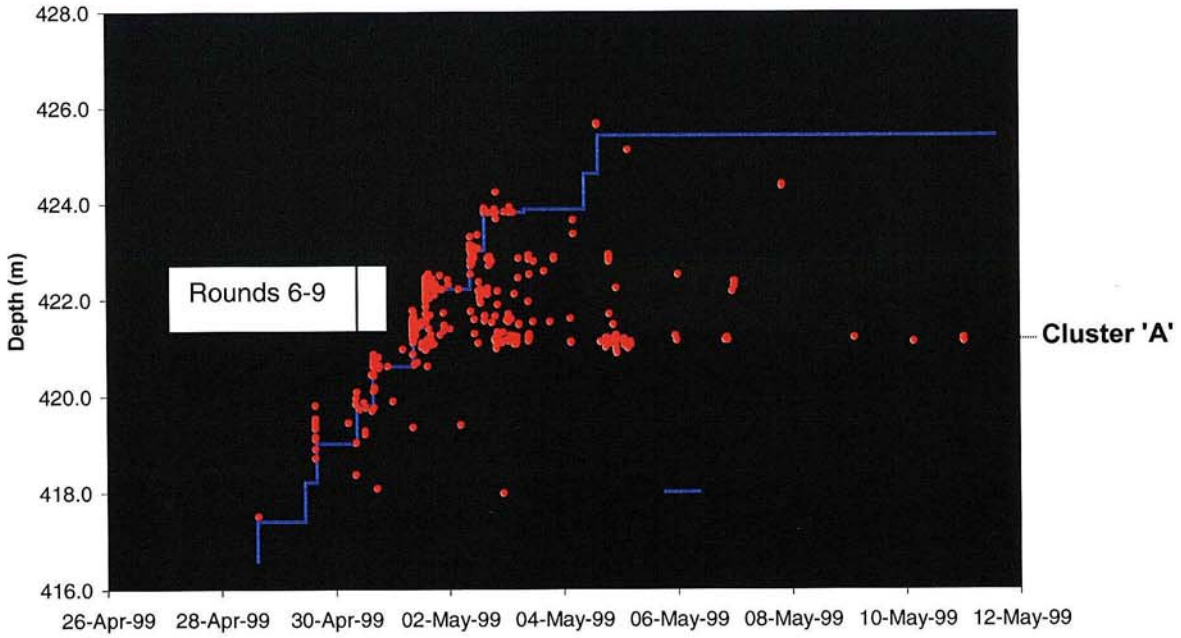

Figure 4-9: *Time dependency of AE activity (red markers). Rounds 6-9 are highlighted along with the depth of Cluster 'A' defined in Figure 4-5.*

During excavation of deposition hole DD0086G01, 37 events have been located in the vicinity of deposition hole DD0092G01. It is uncertain whether this activity is a continuation of that seen as e.g. Cluster 'A' in Figure 4-9 or whether it is triggered as a result of excavating the second deposition hole.

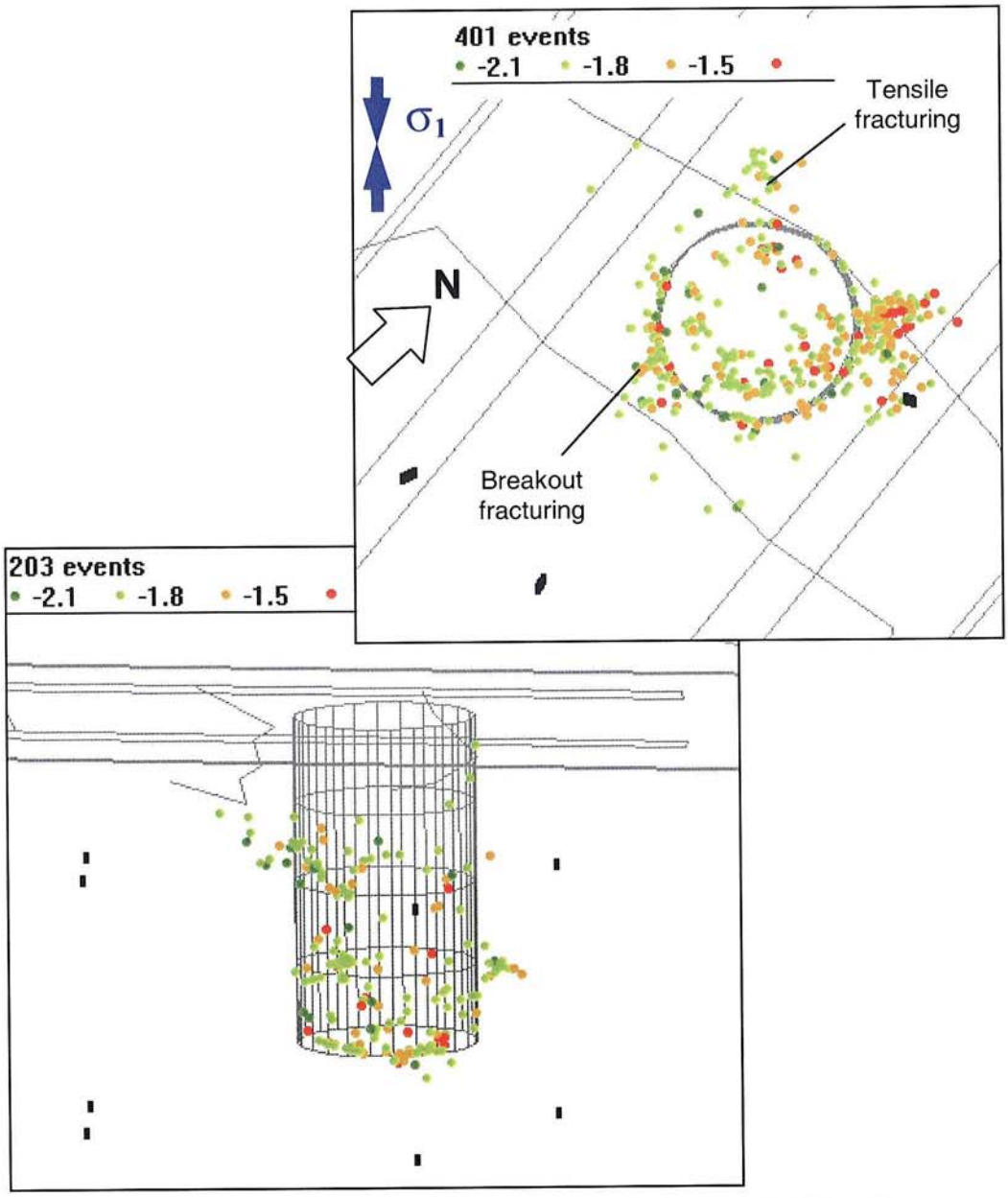

Figure 4-10: *AE locations from monitoring of deposition hole DD0086G01: Upper - All locations; Lower - Locations from Rounds 1-4. The marker colour indicates the relative ultrasonic magnitude. The upper view is in plan and is rotated such that σ_1 is up the page. Lower plot is viewed at an azimuth of 260° East of North and with a plunge of 10° from the horizontal. Black markers show transducer locations.*

4.3 Change in Ultrasonic Properties During Excavation

Figure 4-14 shows examples of the P-wave velocity change during excavation of deposition hole DD0092G01. The four plots show measurements from the four receivers #13 to #16 recording the signal from transmitter #3 (ray path geometries are illustrated). Figure A10 shows similar plots for transmitter #4. All of the shown ray paths skim the perimeter of the deposition hole, passing 2cm from the wall, except transmitter #4 to receiver #16 (Figure A10d) which passes beneath the deposition hole. In each case (except Figure A10d) there is a marked drop in velocity when the deposition hole passes nearest to the ray path (indicated by the red arrow). This drop is generally of the order 10 to 30m.s^{-1} or 0.2 to 0.5% along the entire ray path. The change is rapid and occurs step-like during excavation of the passing round (2-4 hours). This agrees with the AE results, suggesting that the majority of the excavation disturbance occurs during or immediately after excavation. In many of the examples a second drop occurs in the subsequent round indicating that the ray path is further effected by the continuing excavation. In Figure A10d no marked drop in velocity occurs although a gradual decrease of 4m.s^{-1} is observed over the excavation period.

Figure A12 illustrates the change in waveform character observed across a velocity step. Note the change in arrival time that is depicted in Figure 4-14c as a velocity drop. There is also a marked change in amplitude between the two waveforms. P-wave signal amplitudes are shown for all eight ray paths in Figure A13. Every ray path, other than transmitter #4 to receiver #16, shows a drop in amplitude associated with the passing excavation of the order -14dB. The amplitude drop for transmitter #4 to receiver #13 (the longest ray path) decreases the signal to noise sufficiently that the waveform can no longer be processed for velocity (Figure A10a).

For each deposition hole the array geometry is such that in a two-dimensional cross-section of the deposition hole (plan view) there are six possible ray path types illustrated in Figure 4-10. In order to show an overall view of the changes in ultrasonic properties across the array an example of the velocity change is given from each of these categories (Figure A15). For consistency, ray paths have been chosen that pass from a bottom transmitter to a third receiver down the sonde. At distance (approximately 1.5 deposition hole diameters) no step like feature is observed in the velocity change (Figure A15a), however a gradual decrease of 8m.s^{-1} is observed over the excavation

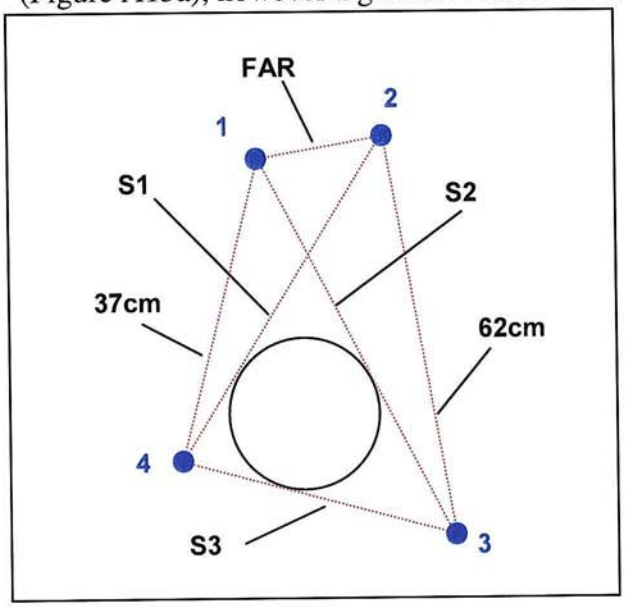

Figure 4-10: *The six possible ray path types in cross-section (plan view). Blue markers indicate the locations of the four ultrasonic sondes. Note that in three dimensions there are 128 possible ray paths between all of the transmitters and receivers down the four sondes. Of the six types there are three sets of skimming ray paths labelled 'S1', 'S2' and 'S3', two sets of ray paths passing at greater distances labelled '37cm' and '62cm'. The final ray path type (labelled 'FAR') does not effectively pass the deposition hole but travels through the rock mass at approximately 1.5 deposition hole diameters.*

period. A similar feature is described in the S-wave velocity and when the ray path passes at 62cm from the deposition hole perimeter (Figure A15e). When the ray path passes at 37cm from the perimeter a distinct step-like change in velocity is observed (Figure A15b). Similarly on skimming ray paths 'S1' and 'S3' (Figure A15c and Figure A15f respectively). However, on skimming ray path 'S2' (Figure A15d), which passes to the NE of the deposition hole, rather than a decrease in velocity a small increase in velocity of 4m.s^{-1} is observed. Similar observations can be made for deposition hole DD0086G01 (Figure A16).

Note that in all cases where S-wave velocities have been obtained, the measured change in velocity is of a similar magnitude and trend to the P-wave velocity. Figure A17 compares the S-wave signal recorded before and after the velocity step. Again note the shift in the waveform measured as the change in velocity of approximately 10m.s^{-1} and the decrease in signal amplitude. This is also of a similar magnitude and trend to the P-wave change (Figure A18).

Obviously, these small changes in transmission properties observed during excavation are complex and depend upon the ray path relative to the deposition hole perimeter. The mean change in velocity observed across all processed skimming ray paths (those in categories 'S1', 'S2' and 'S3' in Figure 4-10) is -15.0m.s^{-1} for deposition hole DD0092G01 and -13.1m.s^{-1} for DD0086G01. Figure 4-13 describes how the mean change in velocity for each ray path category varies over the rock volume. Note that for both holes there is a relatively high change in velocity for ray path category 'S1' compared to the other two skimming categories. Similarly, the category '37cm', which passes through a similar region of the rock volume as 'S1', also has a relatively high velocity change (e.g. Figure A15b).

These variations can be explained in terms of an excavation disturbed zone (where the background stress field is disturbed by the deposition hole excavation) and an excavation damaged zone (where permanent damage is created in the rock volume). It must also be recognised that a velocity change of e.g. -3% is probably caused by the summation of a number of different velocity changes along the ray path (Figure 4-14).

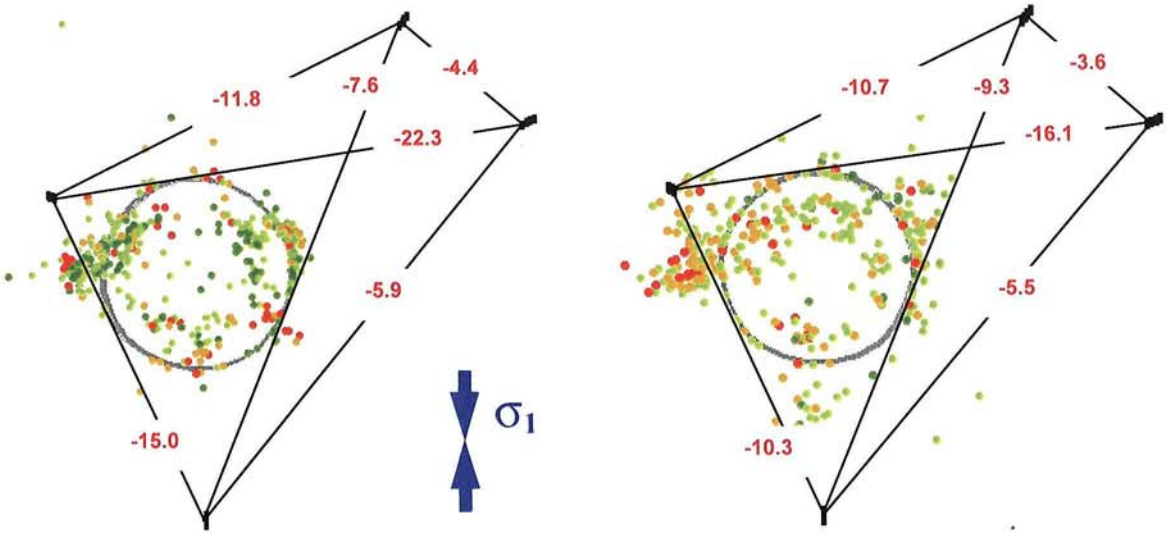

Figure 4-13: *Plan views of the two deposition holes with located AEs: Left - DD0092G01; Right - DD0086G01. The views have been rotated so that σ_1 is up the page. Superimposed onto the plots are the six ray path categories of Figure 4-10 with mean velocity changes indicated.*

These could be increases or decreases due to localised changes in the rock mass.

Small velocity changes (-3 to -6m.s^{-1}) are observed out to as much as 1.5 deposition hole diameters due to the response of the medium to induced changes in stress. This response is due to the preferred closure or opening of pre-existing microcracks depending upon their orientations and the local stress change. No permanent damage is associated with these stresses as no AEs are observed at large distances from the deposition hole. Such a response in measured velocities is well documented in laboratory experiments (e.g. *King et al.*[1997]). This would explain, for instance, why a positive velocity change is observed on Figure A15d even though it is a skimming ray path ('S2') and why this category has on average a relatively small negative velocity change of -8m.s^{-1}. This ray path category contains long ray paths passing through a region expected to be in high compression that in turn causes increased velocities (Figure 4-14). In contrast, ray path category '37cm' has on average a slightly higher negative velocity change (-11m.s^{-1}), or lower absolute velocity, but is not a skimming ray path (e.g. Figure A15b). This ray path passes through a region of low compression or possibly tension. A similar velocity field has been mapped using velocity tomography at the URL (e.g. *Maxwell and Young*[1995]).

Superimposed onto this first velocity change is a second due to permanent damage induced in the rock mass. This has already been observed using AEs and has been shown to exist in localised clusters out to a 20cm radial distance from the deposition hole wall. Only skimming ray paths would be effected by this damage. It should also be noted that due to the specifications of the ultrasonic system, AEs will only be monitored above a certain magnitude. These AEs correspond to the most intense fracturing on the scale of millimetres in dimension. Finer scale cracking, that does not produce as much energy, will not be observed as AEs, however accumulation of this cracking will effect velocities measured along the skimming ray paths. The ray path category with consistently high negative velocity changes is 'S1' (e.g. Figure 4-14 and Figure A10). This category passes through a region of low compressive or possibly tensile stress causing AEs close to the deposition hole perimeter (Figure 4-14). The damage reduces the absolute velocity along the ray path by approximately 15m.s^{-1}. The ray path category 'S3' has on average a slightly lower negative velocity change. This ray path is influenced not only by the region of damage delineated by AE locations (negative

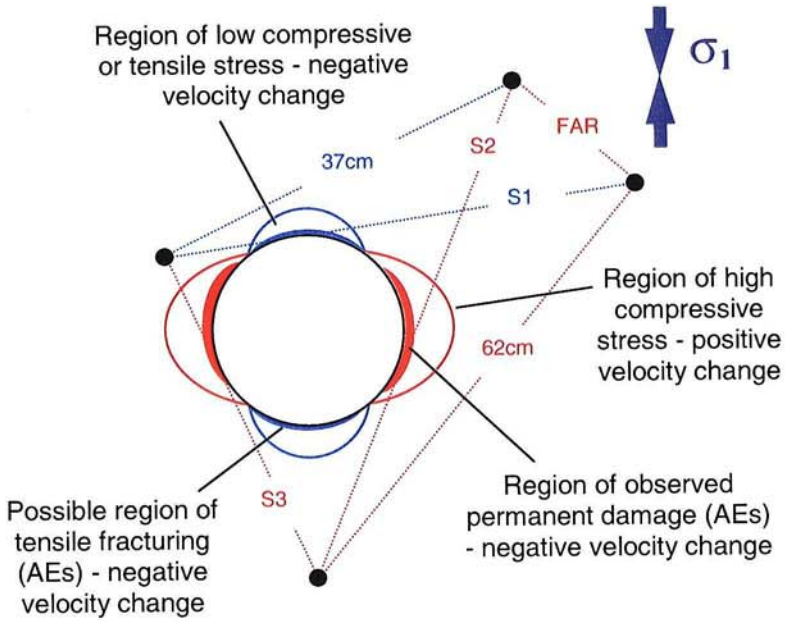

Figure 4-14: *Interpretation of the ultrasonic results in terms of disturbed and damaged regions around the deposition hole. Regions of high stress anomalies are shown as expected from a Kirsch solution and the σ_1 orientation. Also indicated are regions of permanent damage associated with observed AE clustering. Ray paths observed with relatively high velocity decrease are shown in blue.*

change) but also by a region of high compression (positive change).

The velocity measurements can be used to estimate the effect of inducing damage close to the deposition hole on the rock mass properties in this region. It can be shown that the change in velocity over one small section of a ray path (d_D/d_R) is a simple function of the measured change in velocity, Δv over the entire ray path (Equation 1). This assumes the simple model defined in Figure 4-15 and that velocity differences are small compared to the absolute velocities.

$$(v_D - v_R) = \Delta v . \frac{d_R}{d_D}$$

Equation 1

In Equation 1, (v_D-v_R) is the difference between the damaged zone velocity, v_D and the background velocity, v_R. If it's assumed that 5% of the ray path passes through the damaged zone (20cm over a ray path of 4m) then d_D/d_R=0.05. If the measured change in velocity associated with this damaged zone is Δv=-15m.s^{-1}, then (v_D-v_R)=-300m.s^{-1}.

From the results described above, (v_D-v_R) is likely to be similar for P- and S-wave velocities, v_P and v_S respectively. Using v_P = 5900m.s^{-1}, v_S = 3350m.s^{-1} and rock mass density, ρ=2650kg.m^{-3}, then from simple elastic equations the dynamic Young's modulus of the rock mass, E_R=75.1GPa. Using (v_D-v_R)=-300m.s^{-1} from above and assuming the density is not significantly changed gives a dynamic Young's modulus for the damaged region, E_D=63.6GPa. The damaged region hence experiences a 15.3% reduction in Young's modulus.

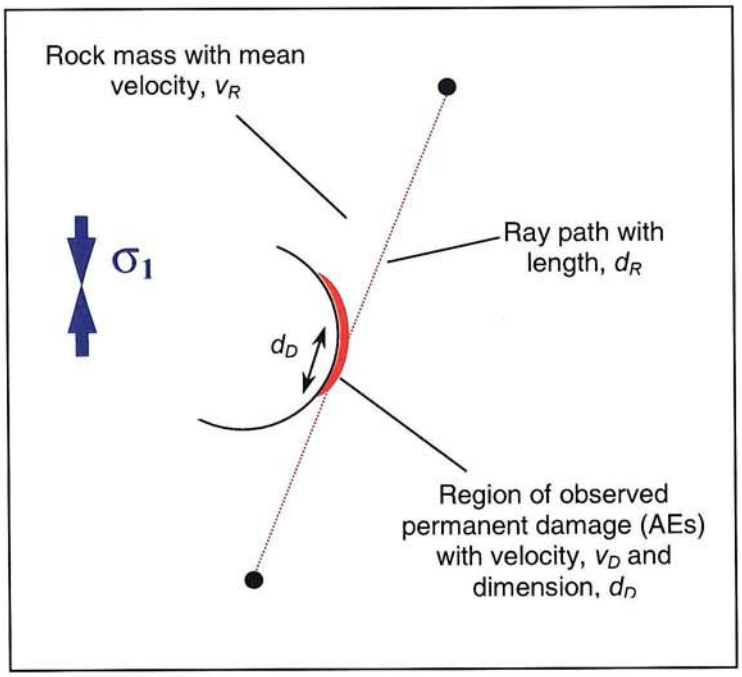

Figure 4-15: *A simple model used for calculating the change in rock properties in the damaged zone (red region) around a deposition hole.*

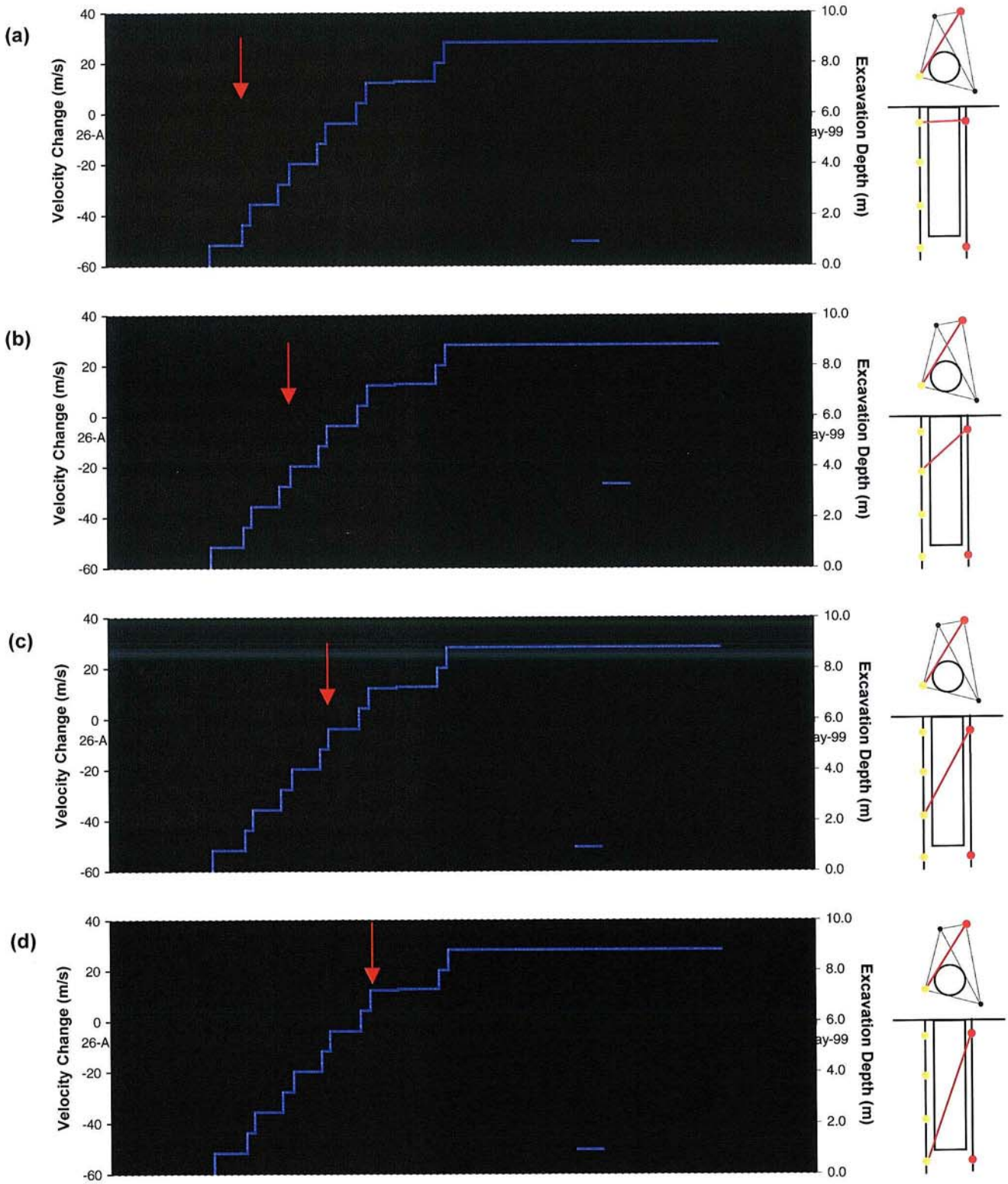

Figure 4-14: *Velocity change measured on four ray paths during excavation of deposition hole DD0092G01: a) transmitter, t_n=3 to receiver r_n=13; b) t_n=3 to r_n=14; c) t_n=3 to r_n=15; d) t_n=3 to r_n=16. Schematic diagrams in the right margin indicate the relative locations of transmitter (red) and receiver (gold). The red arrow indicates the passing depth defined in Figure 3-3.*

5 Results Summary and Conclusions

1. Ultrasonic surveys before excavation of each deposition hole give a mean P-wave velocity of approximately 5900±30m.s^{-1} and a mean S-wave velocity of approximately 3350±60m.s^{-1}. A dynamic Poisson's ratio of 0.26 is hence obtained. An anisotropy of 3% is described in the P-wave measurements. Consistent velocity measurements have been obtained for both monitored deposition holes. The anisotropy could be associated with either the σ_1 direction or a pre-existing microstructure trending NE-SW with a plunge of 40°NW.

2. During the entire monitoring period there were a total of 2746 AE triggers of which 891 have been located with estimated uncertainties <10cm. Activity associated with the first deposition hole (DD0092G01) locates in distinct clusters between 4 and 7m depth and in regions orthogonal to a σ_1 azimuth of 310° East of North. The vast majority of observed fracturing is within 20cm from the deposition hole wall. This activity is associated with high compressive stresses generated by the interaction of the *in situ* stress field with the deposition hole void. Small numbers of AEs are observed parallel to σ_1 in low compressive or tensile conditions. The observed clusters are probably associated with regions of the rock wall that are weaker due to excavation through pre-existing features. As excavation becomes deeper so induced stresses increase beyond the crack-initiation stress for these regions resulting in permanent damage. A possible macroscopic fracture is imaged intersecting the deposition hole. Due to the array specifications the imaged AEs probably occur due to fracturing with dimensions of millimetres. In this case they describe regions where the most intense fracturing is occurring. Cracking on a scale smaller than this may occur but release smaller energy than that locatable by the array. This damage has been imaged by ultrasonic velocity measurements. After completion of excavation the rate of activity decays rapidly in the first 24 hours to <10 triggers per night. These AEs are associated with continued activity in the cluster regions and describe the continued response of the rock mass to the redistributed stress field.

3. For the second deposition hole (DD0086G01) AEs occur at a reduced rate. The majority of fracturing is again constrained within the first 20cm of the deposition hole wall and again locates in regions orthogonal to σ_1. However, the activity is less clustered in this case occurring in a dispersed fashion down the deposition hole length but within 1.5-4.5m excavation depth. This apparent 2m shift in the depth of activity may be due to pre-existing features being less dominant in this case or due to a dissimilar induced stress field. The latter could be a result of the proximity of the first deposition hole. AEs in this damaged region are observed to be strongly time dependent with activity decaying rapidly after the completion of round #4 (3.22m depth) but being reinitiated in the same volume by continued excavation of the deposition hole 12 days later.

4. Over the excavation period P- and S-wave velocities generally describe a small drop in velocity. This change varies from a gradual 4m.s^{-1} observed over the entire excavation period at 1.5 deposition hole diameters distance, to sharp drops of 20-30m.s^{-1} observed over 1-2 rounds for ray paths skimming the deposition hole perimeter. Two effects cause these changes. 1) Changes in the stress field accompany the excavation (Kirsch solution) causing the preferential closure or

opening of fractures in the rock mass. This causes small velocity increases or decreases in regions along the ray path. At 1.5 deposition hole diameters this causes a -4m.s^{-1} change. 2) Accumulation of fracturing close to the deposition hole perimeter, in the damaged region, causes a reduction in velocity. This change is of the order -15m.s^{-1} and occurs rapidly over 3-4 hours during and immediately after excavation of the passing round. This agrees with the observed rate of decay of AE activity. Further decreases in velocity are observed in subsequent rounds suggesting further accumulation of damage and stress redistribution as deposition hole excavation continues. This is also observed in the time dependency of AEs. A -15m.s^{-1} change in velocity measured along the entire ray path results in an estimated change of -300m.s^{-1} in the damaged zone. This yields an estimated 15% drop in Young's modulus for the damaged rock mass.

6 Recommendations

1. **Relationship between AEs and the stress field.** It would be advisable to model stress magnitudes in the vicinity of each deposition hole. This modelling could be validated by stress measurements performed in the CRT. The aim would be to analyse the stress distribution around deposition hole DD0092G01 and relate this to observed AE distributions and pre-existing features that intersect the deposition hole perimeter. Stress magnitudes can then be obtained for the AE source locations in a similar manner to that performed by e.g. *Falls and Young*[1996] and a failure criteria established for the observed fracturing. It would be interesting to observe the stress effect of the first deposition hole on the excavation of the second deposition hole, DD0086G01. Does the proximity of the first deposition hole effect the stress distribution in the second deposition hole's volume that in turn causes some of the observed differences in AE activity? What happens when a row of three deposition holes is then used in the models? This may have a considerable bearing on how deposition holes are located relative to one another in a repository.

2. **AE mechanism and cluster location analysis.** A source mechanism analysis (e.g. *Pettitt et al.*[1998]) should be performed for some of the AE data. This would result in the type and orientation of fracturing in the damaged region. This should be related to the stress analysis suggested above and may delineate fracture pathways through the damaged zone. The AE data would need to be carefully chosen and probably limited to early rounds. Data from deposition hole DD0086G01 round #4 (Figure 4-10) gives an ideal opportunity. The resolution of source locations from clustering in deposition hole DD0092G01 could be enhanced using a relative location technique or similar. This may result in the observed features being better distinguished and more comparable to features physically observed in the field. For instance, do all features intersected by the deposition hole cause fracturing to be observed ultrasonically, or do only features that are preferentially orientated to the stress field cause an effect? This may give a constraint on the design of deposition hole locations relative to known features in a repository.

References

ASC, *Ultrasonic Monitoring During the Excavation of Deposition Boreholes in the Retrieval Tunnel: Trip Report and Data Description*, SKB/Äspö 02, Applied Seismology Consultants Ltd, Shrewsbury, UK, 1999.

Falls, S.D., *Ultrasonic Imaging and Acoustic Emission Studies of Microcrack Development in Lac Du Bonnet Granite*, PhD thesis, Department of Geological Sciences, Queen's University, Kingston, Ontario, Canada, 1993.

Falls, S.D., and R.P. Young, Examination of the excavation disturbed zone in the Swedish ZEDEX tunnel using acoustic emission and ultrasonic velocity measurements, in *Proceedings of Eurock '96, Turin, Italy, 1996*,Balkema, Rotterdam, pp. 1337-1344, 1996.

Falls, S.D., and R.P. Young, Acoustic emission and ultrasonic-velocity methods used to characterise the excavation disturbance associated with deep tunnels in hard rock, *Tectonophysics, 289*, 1-15, 1998.

Falls, S.D., and R.P. Young, *Acoustic Emission Monitoring of the Drill and Blast Drift*, Internal Research Report, Applied Seismology and Rock Physics Laboratory, Keele University, Staffordshire, U.K., May 1995.

Falls, S.D., and R.P. Young, *Observations from Acoustic Emission Monitoring of the TBM Drift*, Internal Research Report, Applied Seismology and Rock Physics Laboratory, Keele University, Staffordshire, U.K., October 1994.

King, M.S., A. Shakeel, and N.A. Chaudhrey, Acoustic wave propagation and permeability in sandstones with systems of aligned cracks, in *Developments in Petrophysics*, edited by M.A. Lovell, and P.K. Harvey,Geological Society Special Publication No. 122, pp. 69-85, 1997.

Leijon, B., *Summary of Rock Stress Data from Äspö*, Äspö Hard Rock Laboratory Progress Report 25-95-15, Swedish Nuclear Fuel and Waste Management Company, Sweden, 1995.

Maxwell, S.C., and R.P. Young, A controlled in-situ investigation of the relationship between stress, velocity and induced seismicity, *Geophys. Res. Lett.*, 22, 1049-1052, 1995.

Pettitt, W.S., R.P. Young, and J.R. Marsden, Investigating the mechanics of microcrack damage induced under true-triaxial unloading, Paper No. 47319, in *SPE/ISRM Eurock '98*,Society of Petroleum Engineers Inc., pp. 509-517, 1998.

Read, R.S., and C.D. Martin, *Technical Summary of AECL's Mine-by Experiment Phase 1: Excavation Response*, AECL, Whiteshell Laboratories, Pinawa, Manitoba, Canada, February 1996.

SKB, *Äspö Hard Rock Laboratory: Current Research Projects 1998*, Swedish Nuclear Fuel and Waste Management Company, Sweden, 1999.

Young, R.P., and D.S. Collins, Monitoring an experimental tunnel seal in granite using acoustic emission and ultrasonic velocity, in *Rock Mechanics for Industry, Proceedings of the 37th U.S. Rock Mechanics Symposium, Vail, Colorado*, edited by Amadei, Kranz, Scott, and Smeallie,Balkema, Rotterdam, 1999.

Young, R.P., C.D. Martin, R. Murdie, J. Alcott, S. Falls, I. Stimpson, and S. Yazici, *Numerical Modelling, Acoustic Emission and Velocity Studies of the Excavation Disturbed Zone at the Hard Rock Laboratory*, Äspö Hard Rock Laboratory Technical Note, Swedish Nuclear Fuel and Waste Management Company, Sweden, 1996.

Appendix

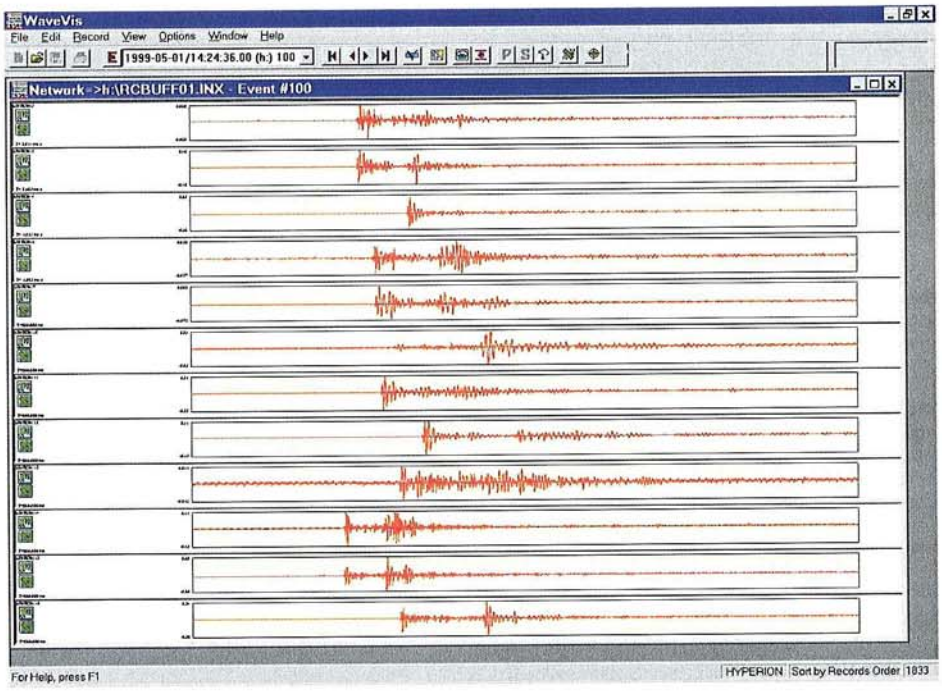

Figure A1: *Waveforms from an AE recorded shortly after cessation of drilling of deposition hole DD0092G01 at 5.83m depth (Round #7).*

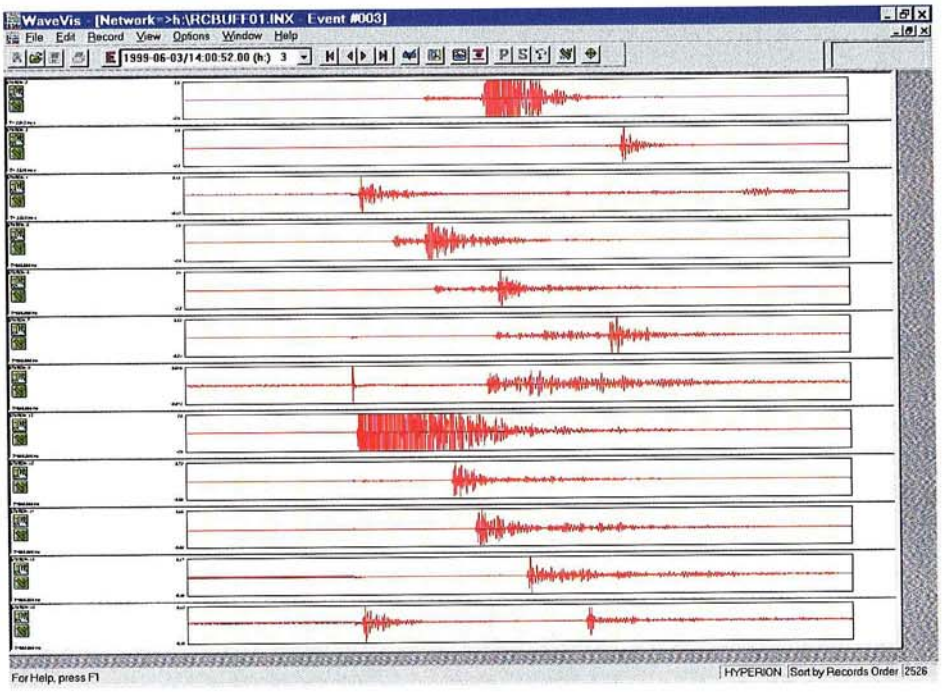

Figure A2: *Example waveforms from an ultrasonic survey conducted after excavation of deposition hole DD0086G01.*

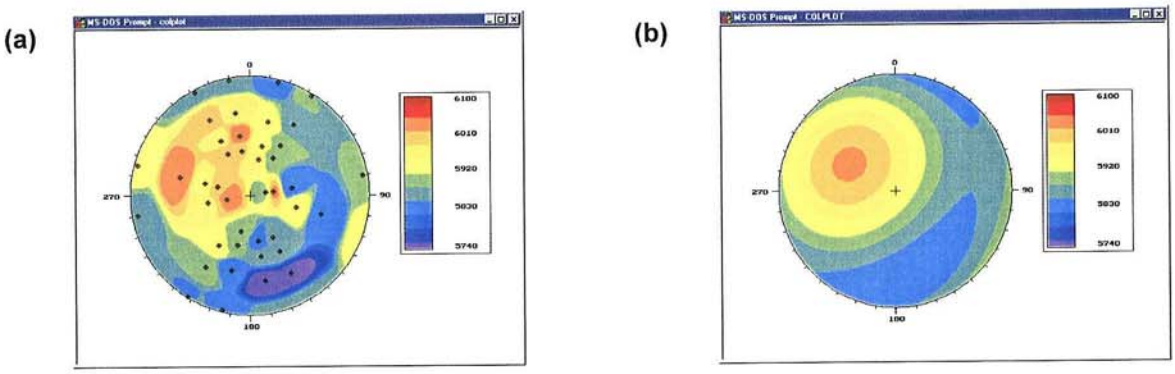

Figure A4: a) *Measured velocities from the reference survey (17th May at 0100) used for deposition hole DD0086G01.* ***b)*** *Three-dimensional anisotropy fit to the data.*

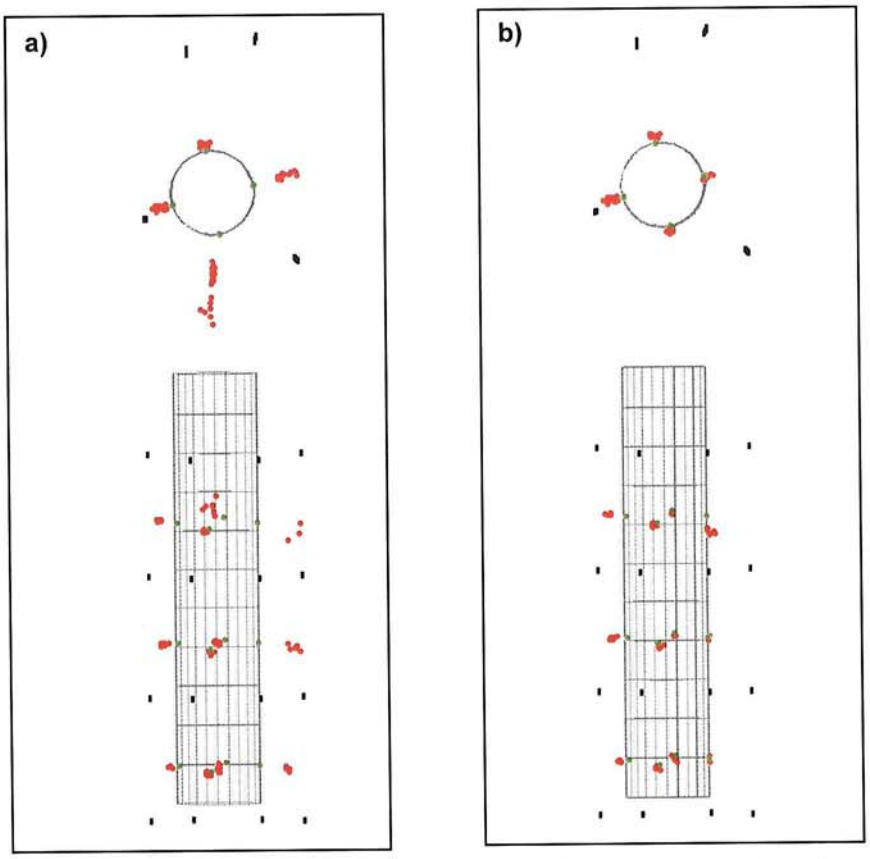

Figure A5: *Locations of calibration shots (red markers) performed in deposition hole DD0092G01, used to optimise and evaluate the processing procedure for AEs.* ***a)*** *Unconstrained locations.* ***b)*** *Constrained locations. Green markers indicate the true locations of the shots calculated from survey points. Top plots are in plan; bottom plots are in cross-section.*

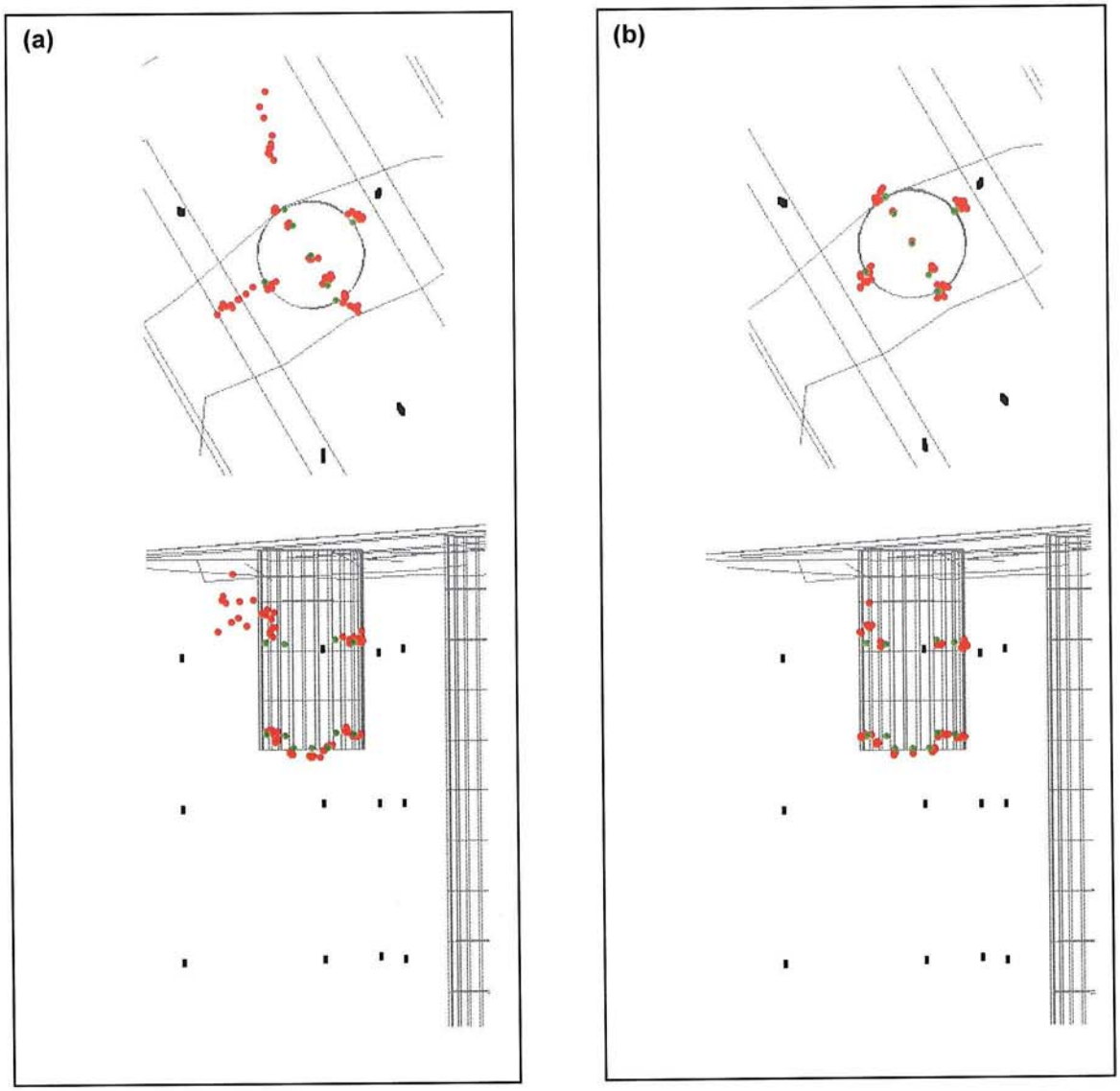

Figure A6: *Locations of calibration shots (red markers) performed in deposition hole DD0086G01, used to optimise and evaluate the processing procedure for AEs.* ***a)*** *Unconstrained locations.* ***b)*** *Constrained locations. Green markers indicate the true locations of the shots calculated from survey points. Top plots are in plan; bottom plots are in cross-section.*

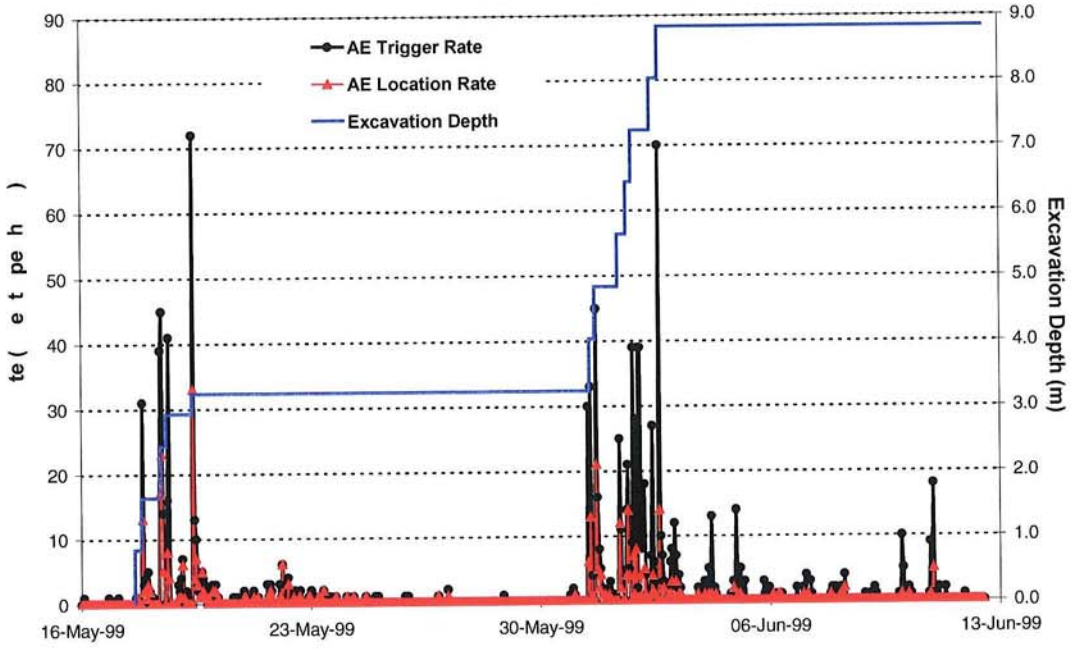

Figure A8: *AE rate through excavation of deposition hole DD0086G01. Both the system trigger rate (black) and location rate (red) are shown.*

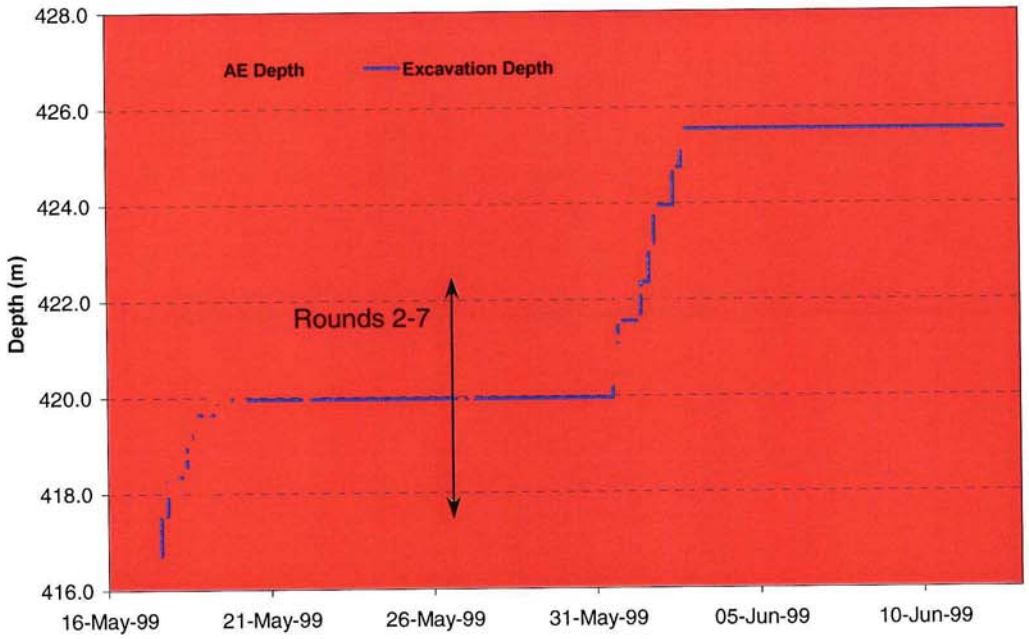

Figure A7: *Time dependency of AE activity (red markers) for deposition hole DD0086G01.*

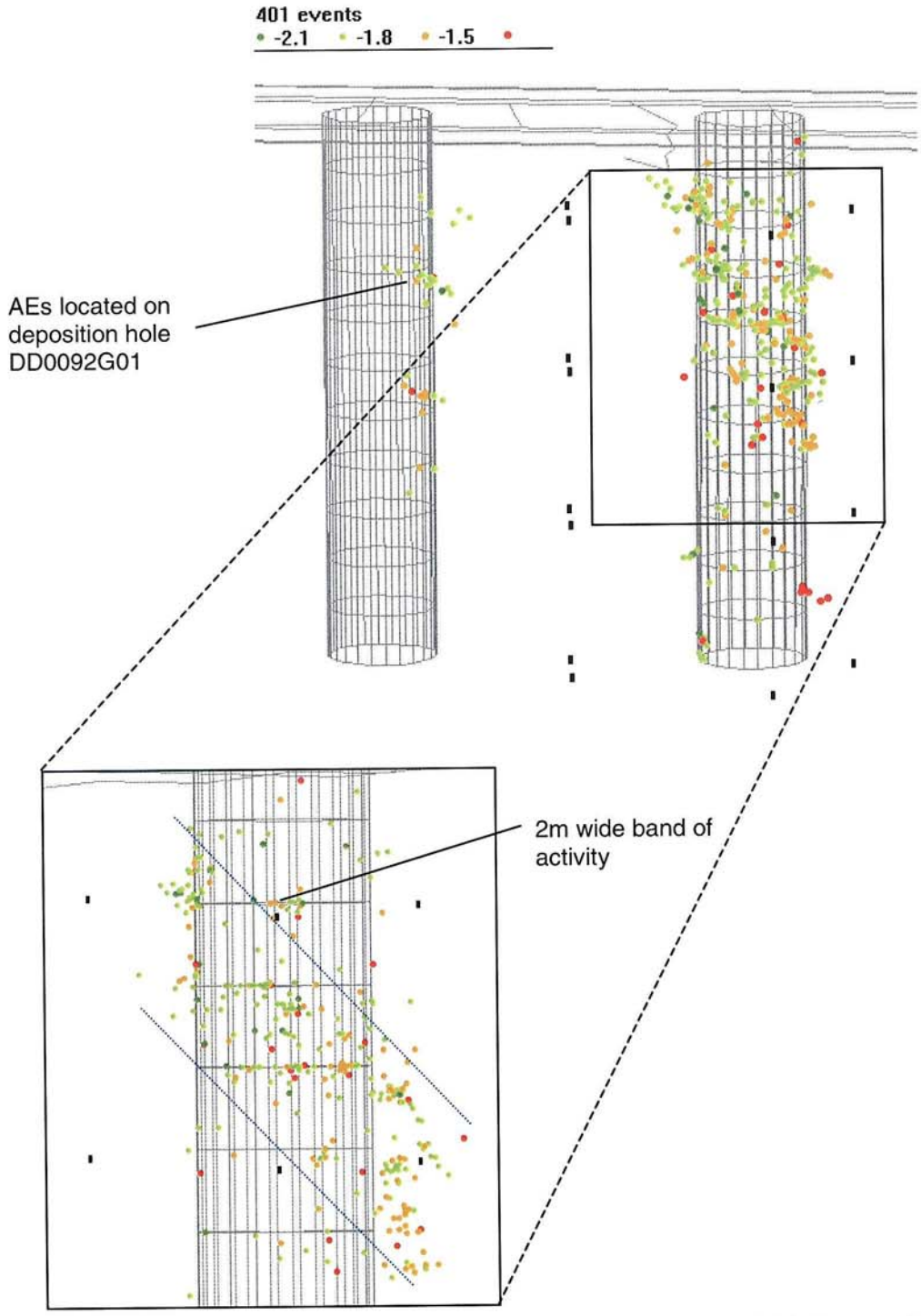

Figure A11: *AE locations from monitoring of deposition hole DD0086G01. The marker colour indicates the relative ultrasonic magnitude. The upper plot is viewed at an azimuth of 260° East of North and with a plunge of 10° from the horizontal. The lower view is in the direction of σ_1 (azimuth of 310° East of North and with a plunge of 0°). Black markers show transducer locations.*

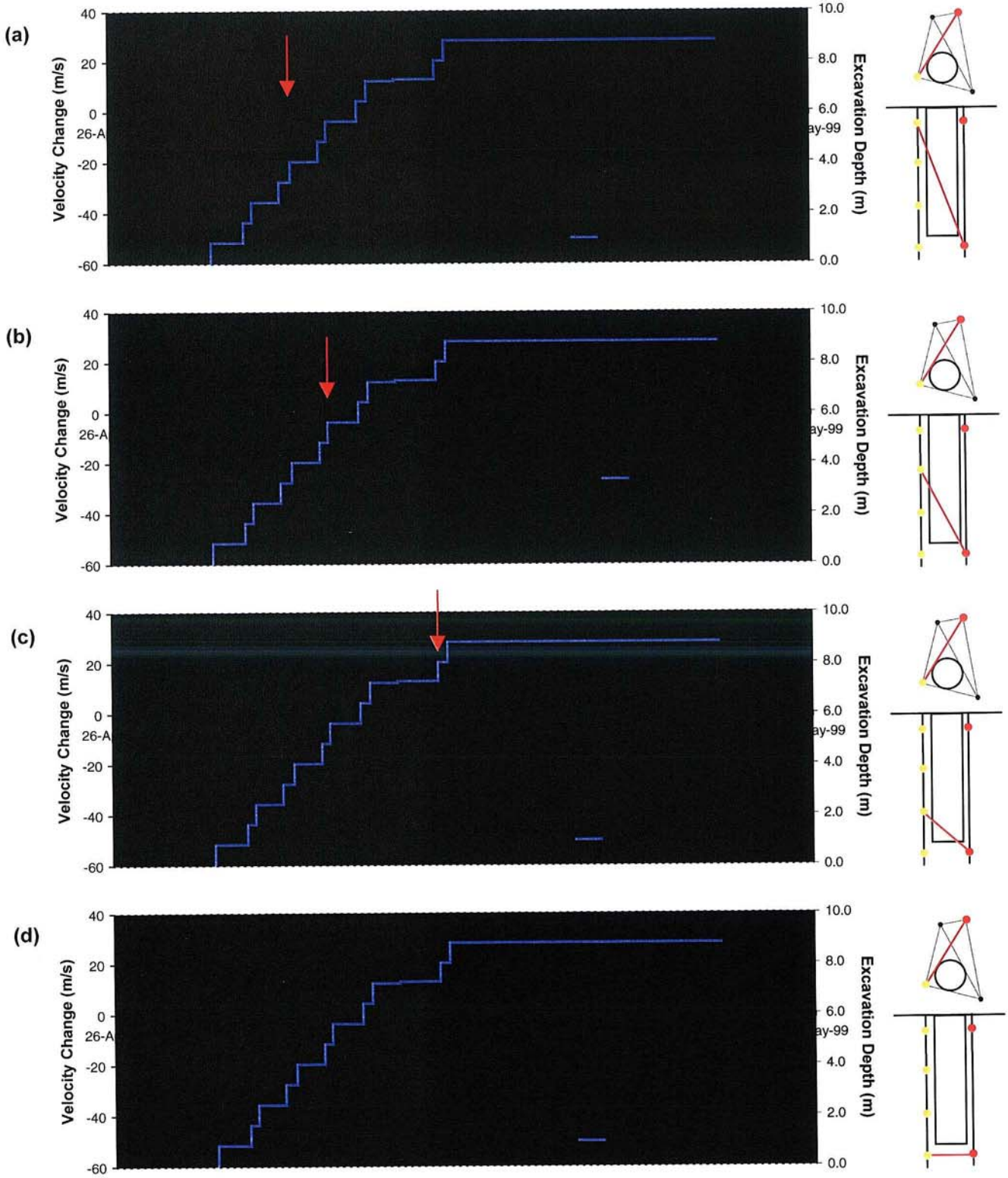

Figure A10: *Velocity change measured on four ray paths during excavation of deposition hole DD0092G01: a) transmitter, t_n=4 to receiver r_n=13; b) t_n=4 to r_n=14; c) t_n=4 to r_n=15; d) t_n=4 to r_n=16. Schematic diagrams in the right margin indicate the relative locations of transmitter (red) and receiver (gold). The red arrow indicates the passing depth defined in Figure 3-3.*

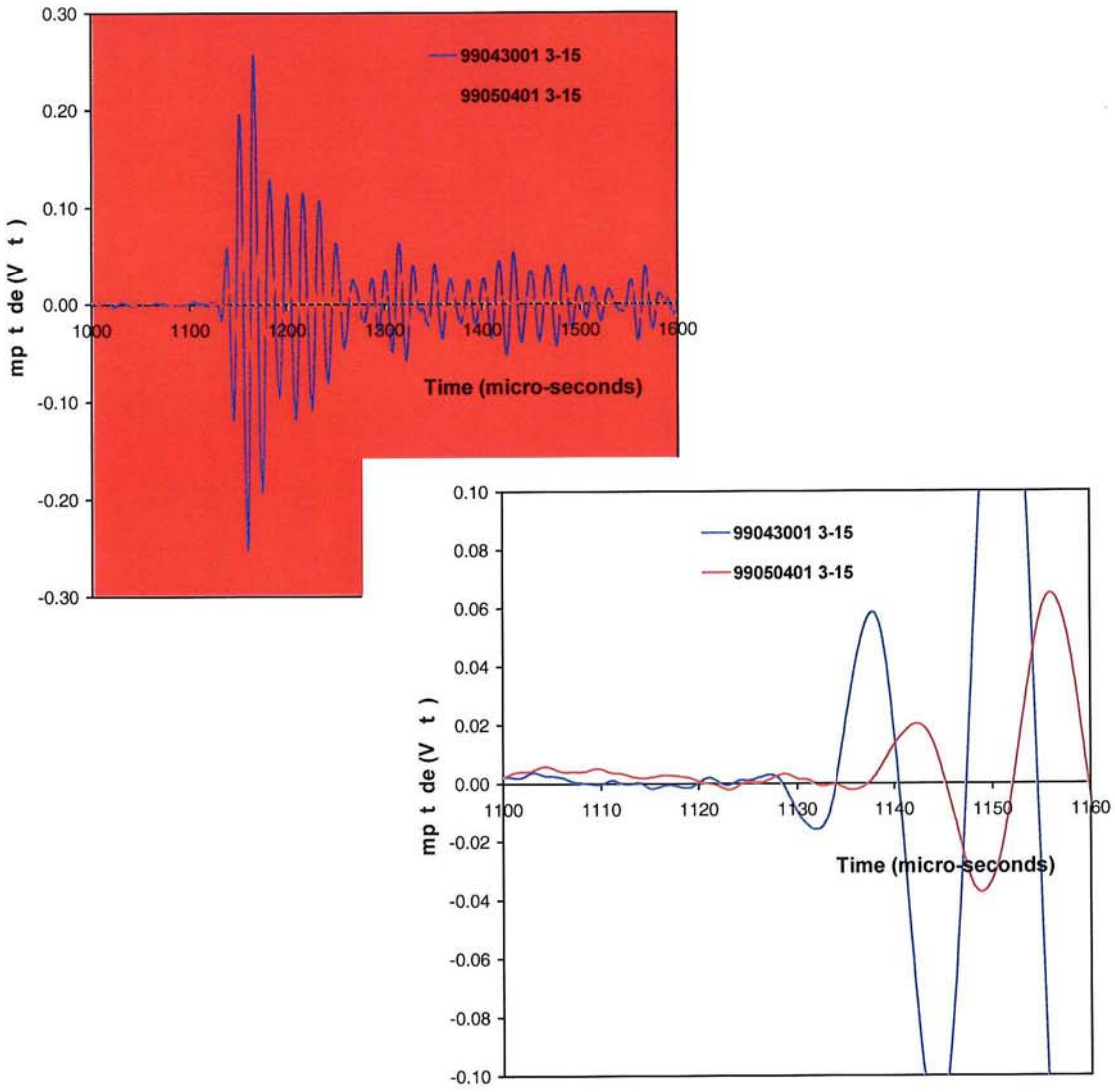

Figure A12: *Recorded signals on receiver #15 from transmitter #3 from before (blue) and after (red) the observed velocity step (Figure 4-14c). The lower plot is a time-amplitude expansion of the P-wave arrival.*

(a)

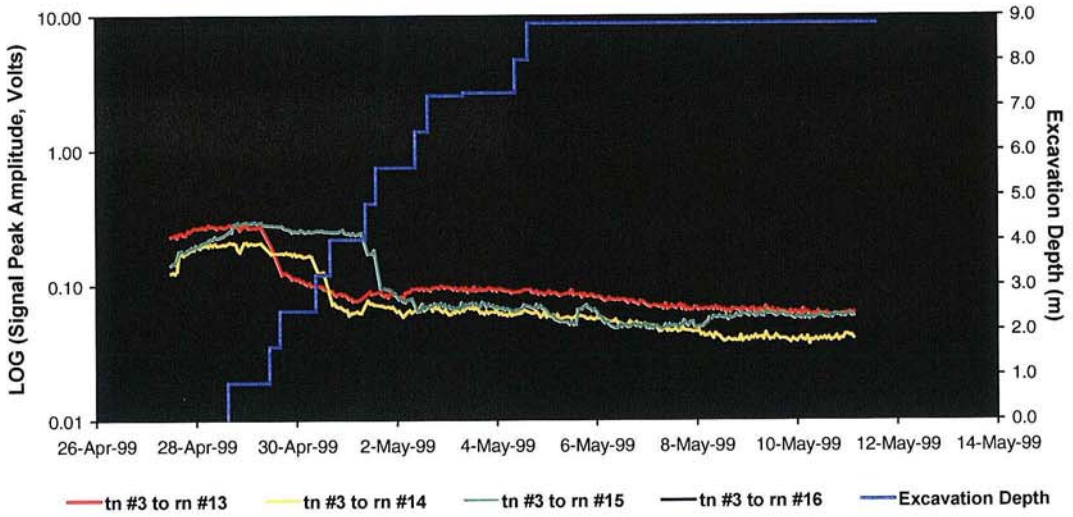

(b)

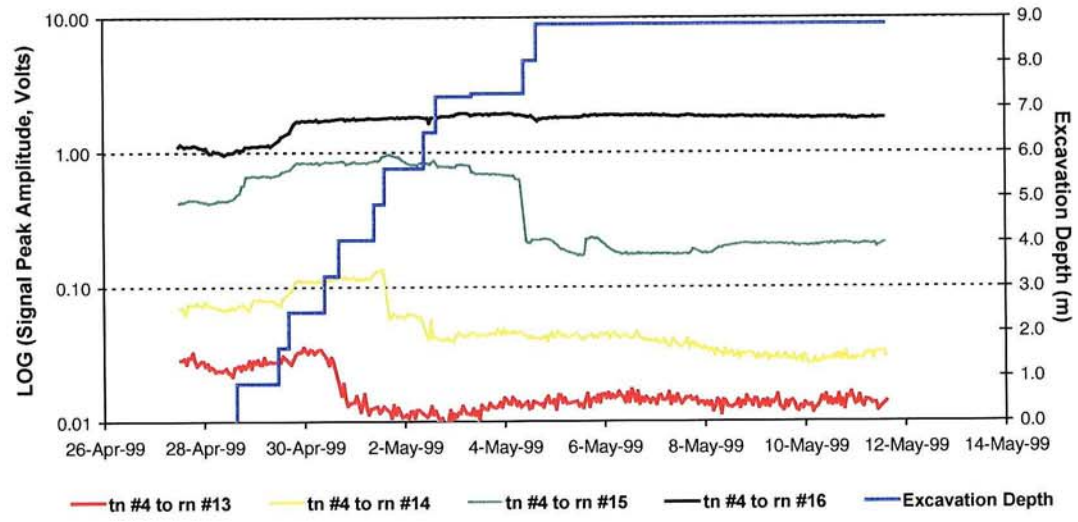

Figure A13: *Change in P-wave signal amplitudes for the ray paths shown in* ***a)*** *Figure 4-14 and* ***b)*** *Figure A10.*

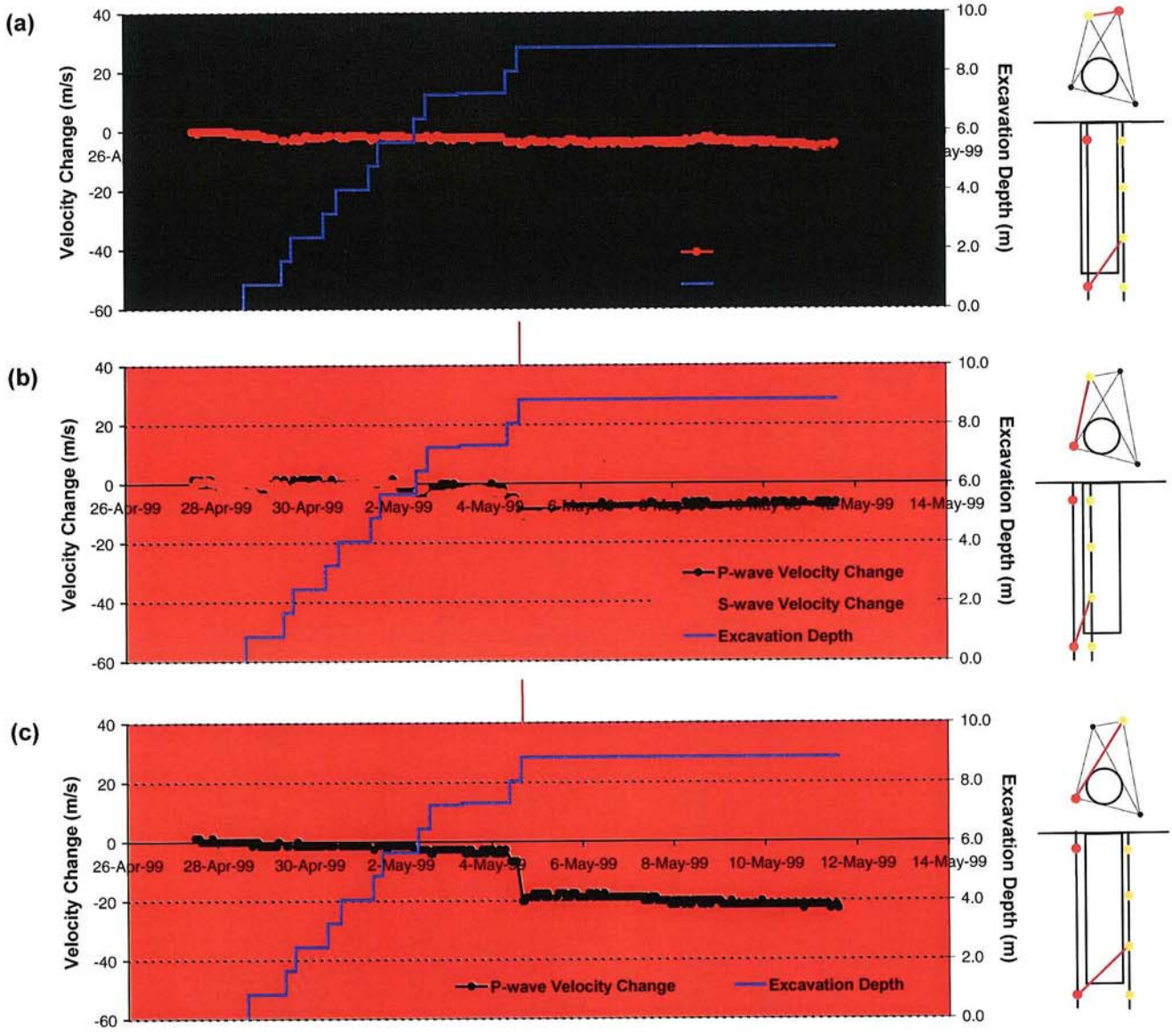

Figure A15: *Examples of velocity change measured on the six ray path types (continued overleaf) defined in Figure 4-10 during excavation of deposition hole DD0092G01:* ***a)*** *'FAR' - transmitter, t_n=2 to receiver r_n=7;* ***b)*** *'37cm' - t_n=8 to r_n=3;* ***c)*** *'S1' - t_n=8 to r_n=7;* ***d)*** *'S2' - t_n=6 to r_n=3;* ***e)*** *'62cm' - t_n=6 to r_n=7;* ***f)*** *'S3' - t_n=6 to r_n=15. Schematic diagrams in the right margin indicate the relative locations of transmitter (red) and receiver (gold). The red arrow indicates the passing depth defined in Figure 3-3.*

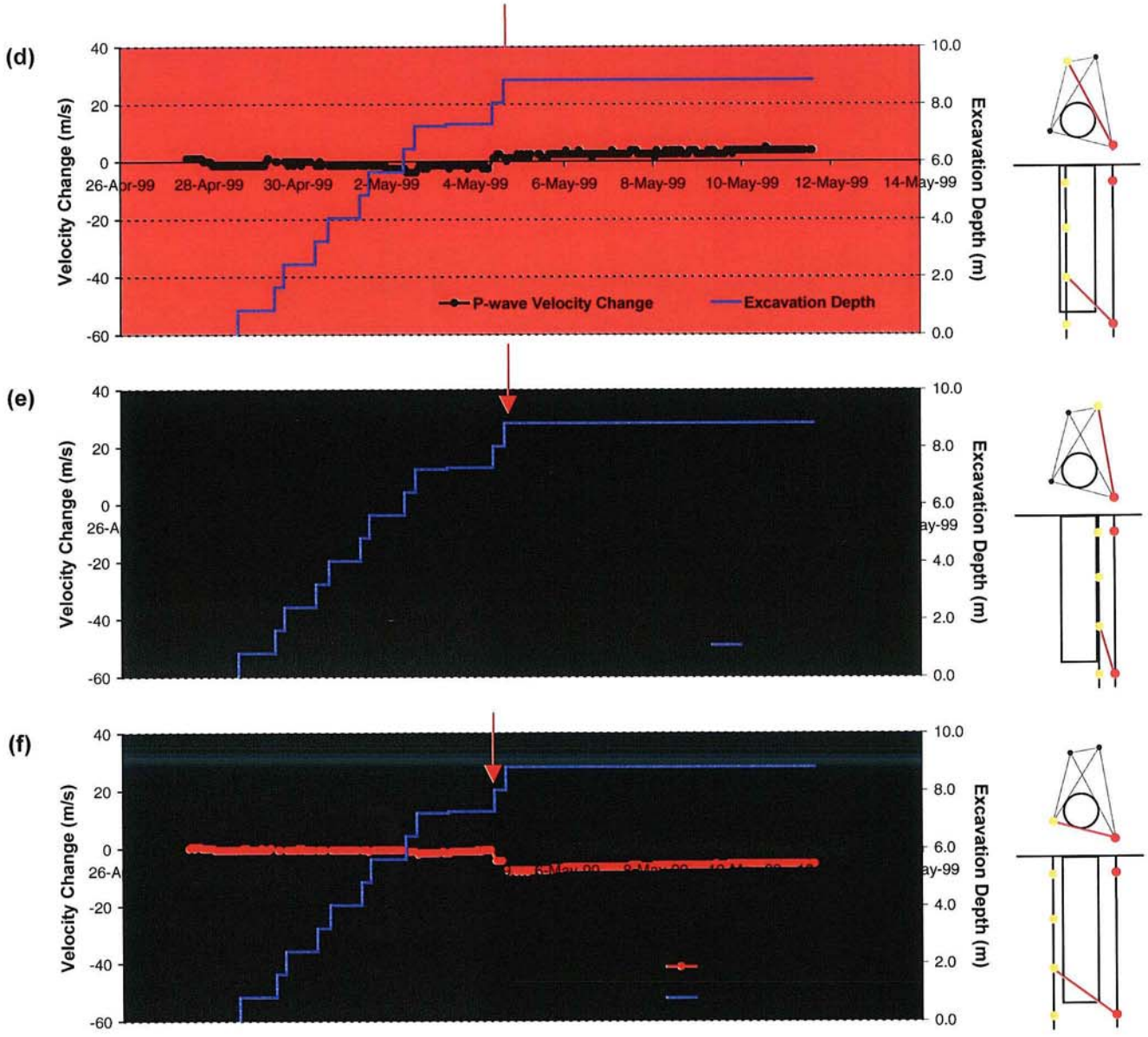

Figure continued from previous page.

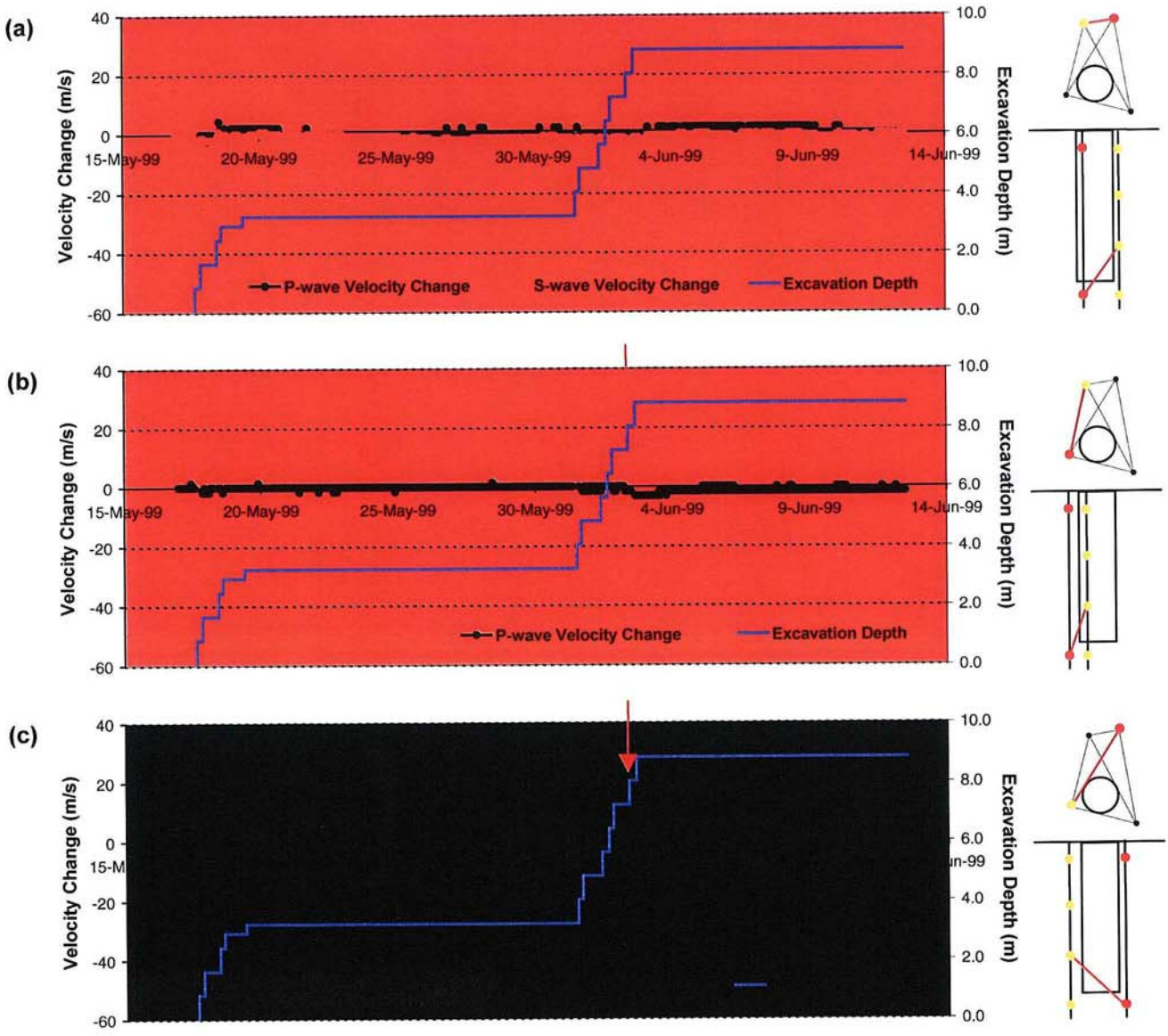

Figure A16: *Examples of velocity change measured on the six ray path types (continued overleaf) defined in Figure 4-10 during excavation of deposition hole DD0086G01:* ***a)*** *'FAR' - transmitter, t_n=2 to receiver r_n=7;* ***b)*** *'37cm' - t_n=8 to r_n=3;* ***c)*** *'S1' - t_n=4 to r_n=15;* ***d)*** *'S2' - t_n=6 to r_n=3;* ***e)*** *'62cm' - t_n=6 to r_n=7;* ***f)*** *'S3' - t_n=6 to r_n=15. Schematic diagrams in the right margin indicate the relative locations of transmitter (red) and receiver (gold). The red arrow indicates the passing depth defined in Figure 3-3.*

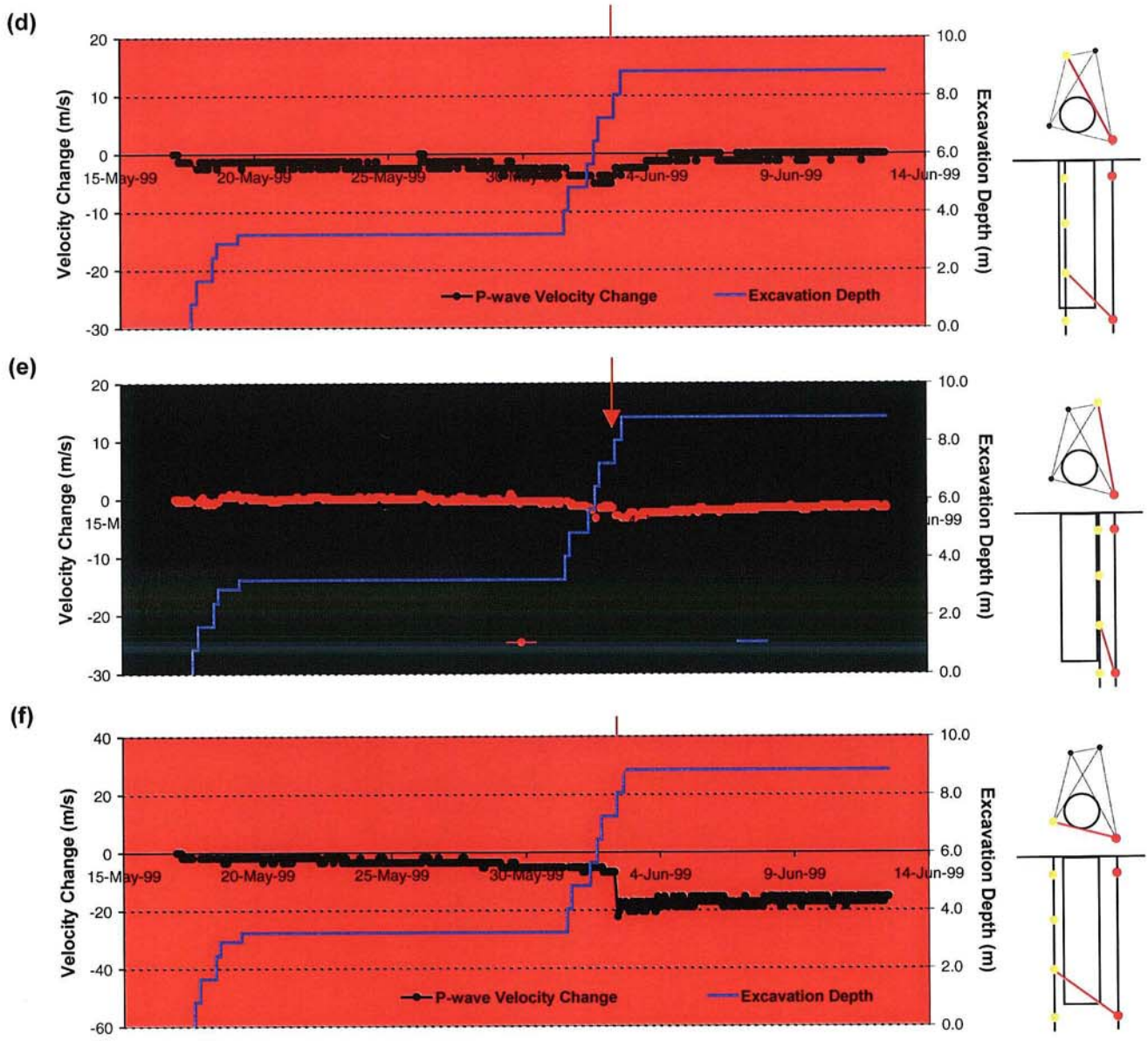

Figure continued from previous page.

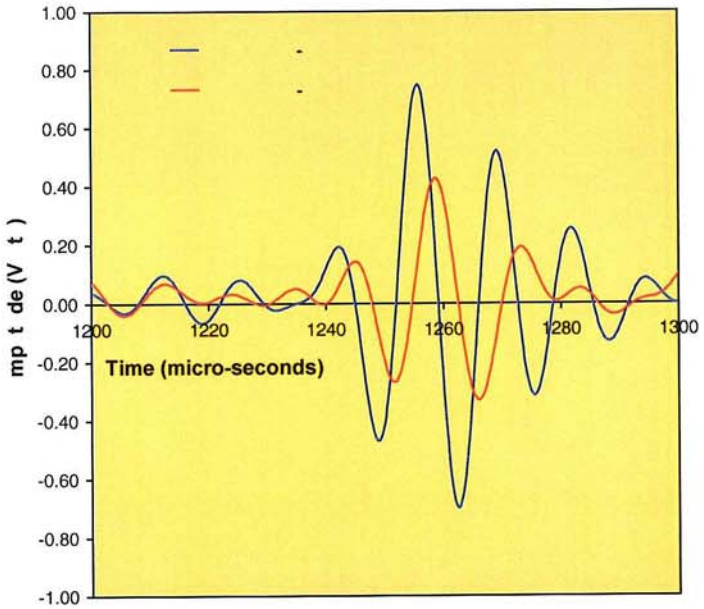

Figure A17: *Change in the S-wave signal for transmitter #6 to receiver #15 due to excavation of deposition hole DD0092G01. Before excavation - blue; after excavation - red. The associated change in velocity is described in Figure A15f and the change in amplitude in Figure A18.*

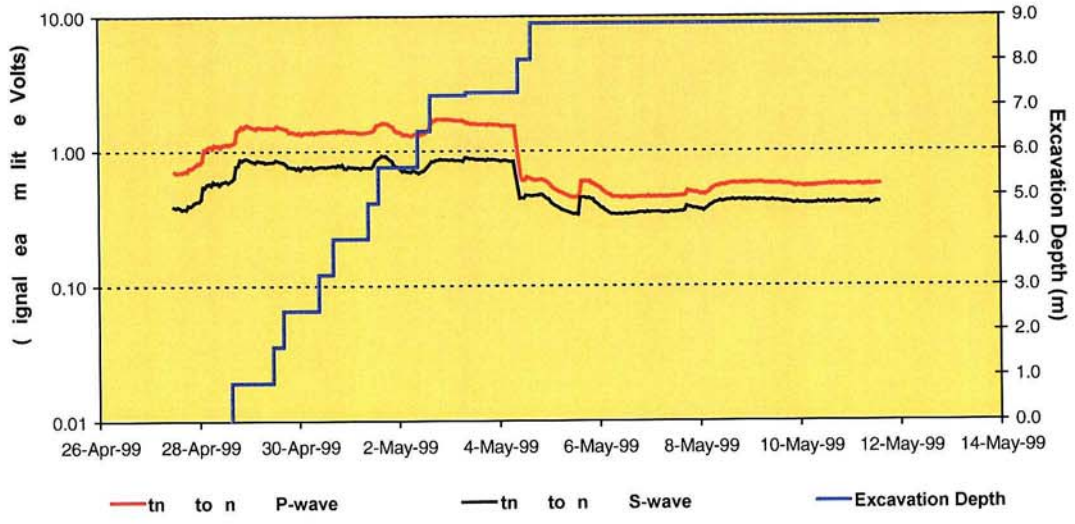

Figure A18: *Change in measured signal peak amplitude for both the P-wave (red) and S-wave (black) for transmitter #6 to receiver #15 during excavation of deposition hole DD0092G01.*